Supporting Information:

Structural Chemistry, Flexibility and CO_2 Adsorption Performance of Alkali Metal Forms of Merlinoite with Framework Si/Al Ratio of 4.2

Elliott L. Bruce,[1] Veselina M. Georgieva,[1] Maarten C. Verbraeken,[2] Claire Murray,[3] Ming-Feng Hsieh,[4] William J. Casteel, Jr.,[5] Alessandro Turrina,[4] Stefano Brandani[2] and Paul A. Wright[1,*]

1. EaStCHEM School of Chemistry, University of St Andrews, Purdie Building, North Haugh, St Andrews, UK.

2. School of Engineering, University of Edinburgh, The King's Buildings, Edinburgh, UK

3. Diamond Light Source, Harwell Science and Innovation Campus, Didcot, UK

4. Johnson Matthey Technology Centre, Chilton P.O. Box 1, Belasis Avenue, Billingham, UK

5. Air Products and Chemicals Inc., 7201 Hamilton Blvd., Allentown, PA18195 USA

* Email: paw2@st-andrews.ac.uk

Contents

S1. SEM Images

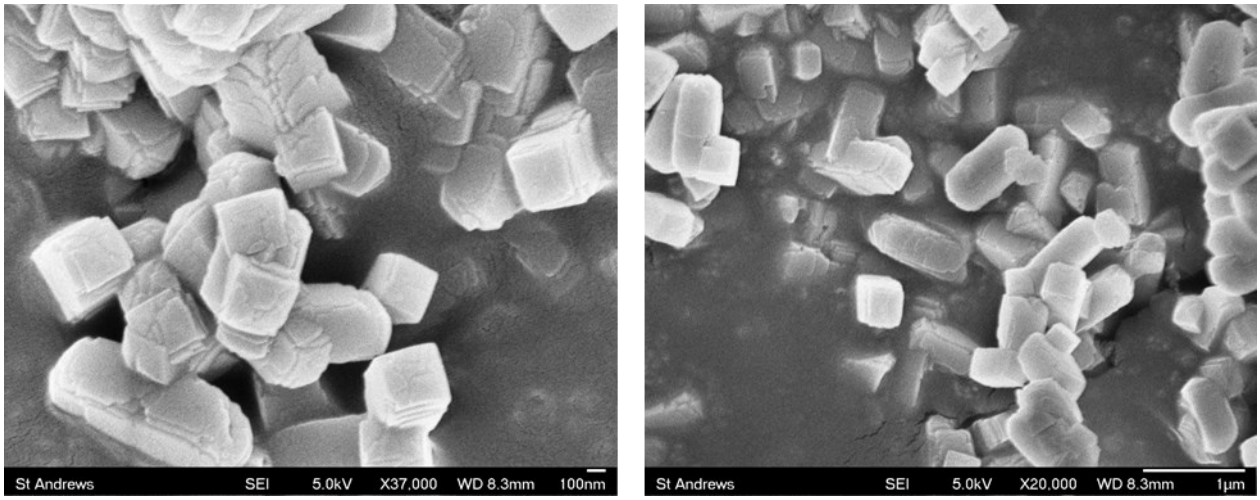

Figure S1.1. SEM micrographs of $K_{5.2}TEA_{1.0}$-MER (Si/Al = 4.2) zeolite sample.

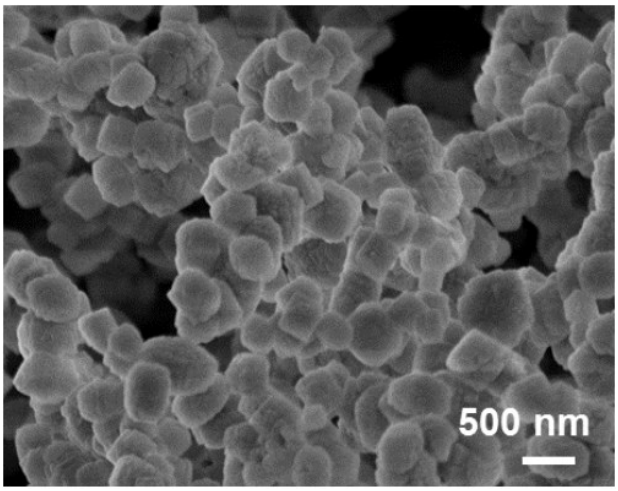

Figure S1.2. SEM micrographs of $K_{6.2}TEA_{0.5}$-MER (Si/Al = 3.8) zeolite sample.

S2. Structural response to dehydration

S2.1. Pure Cation MER materials

Table S2.1. Crystallography of pure cation MER materials in this work.

Sample	**$Cs_{6.2}$-MER**	**$K_{6.2}$-MER**
Unit Cell	$Cs_{5.9}[Si_{25.8}Al_{6.2}O_{64}]$	$K_{6.1}[Si_{25.8}Al_{6.2}O_{64}]$
T (K)	298	298
Space Group	*Pmmn*	*Pmmn*
X-ray Source	I11	I11
λ (Å)	0.826398	0.826398
***a* (Å)**	13.794(1)	13.950(1)
***b* (Å)**	13.776(1)	13.894(1)
***c* (Å)**	9.940(1)	9.831(1)
***V* (Å^3)**	1889(1)	1905(1)
R_{wp}	5.5	2.4
R_p	3.8	1.9
χ^2	54	24

Table S2.2. Cation site distribution determined by Rietveld refinement. Site labelling (I, I', Ia, IIa, IIb, III, III') is as described in the text, and for each sample the multiplicity (M), fractional occupancy and number of cations per unit cell are given.

Sample	**I**			**I'**			**IIa**			**IIb**		
	M	frac. occ.	atoms/uc	M	frac. occ.	atoms/uc	M	frac. occ.	atoms/uc	M	frac. occ.	atoms/uc
$K_{6.2}$-MER	2	0.32(1) K	0.6(1) K	2	0.30(1) K	0.6(1) K	4	0.58(1) K	2.3(1) K	4	0.64(1) K	2.6(1) K
$K_{5.7}Na_{0.5}$-MER	2	0.22(1) K	0.4(1) K	2	0.30(1) K	0.6(1) K	4	0.47(1) K	1.9(1) K	4	0.61(1) K	2.4(1) K
$K_{5.2}Na_{1.0}$-MER				2	0.81(2) K	1.6(1) K	4	0.37(1) K	1.5(1) K	4	0.78(1) K	3.1(1) K
$K_{4.2}Na_{2.0}$-MER				2	0.39(1) K	0.8(1) K	4	0.41(1) K	1.6(1) K	4	0.46(1) K	1.8(1) K
$K_{3.2}Na_{3.0}$-MER	2	0.45(2) Na	0.9(1) Na	2	0.30(1) Na	0.6(1) Na	4	0.37(1) K	1.5(1) K	4	0.38(1) K	1.5(1) K
$K_{2.2}Na_{4.0}$-MER				2	0.60(2) Na	1.2(1) Na	4	0.40(1) K	1.6(1) K	4	0.70(1) Na	2.8(1) Na
$K_{1.2}Na_{5.0}$-MER	2	0.67(3) Na	1.3(1) Na	2	0.09(3) Na	0.2(1) Na	4	0.31(1) K	1.2(1) K	4	0.66(2) Na	2.6(1) Na

Sample	Ia			IIa			III			III'		
	M	frac. occ.	atoms/uc	M	frac. occ.	atoms/uc	M	frac. occ.	atoms/uc	M	frac. occ.	atoms/uc
$Cs_{6.2}$-MER	2	0.80(1) Cs	1.6(1) Cs	4	0.37(1) Cs	1.5(1) Cs	2	0.64(1) Cs	1.3(1) Cs	2	0.73(1) Cs	1.5(1) Cs

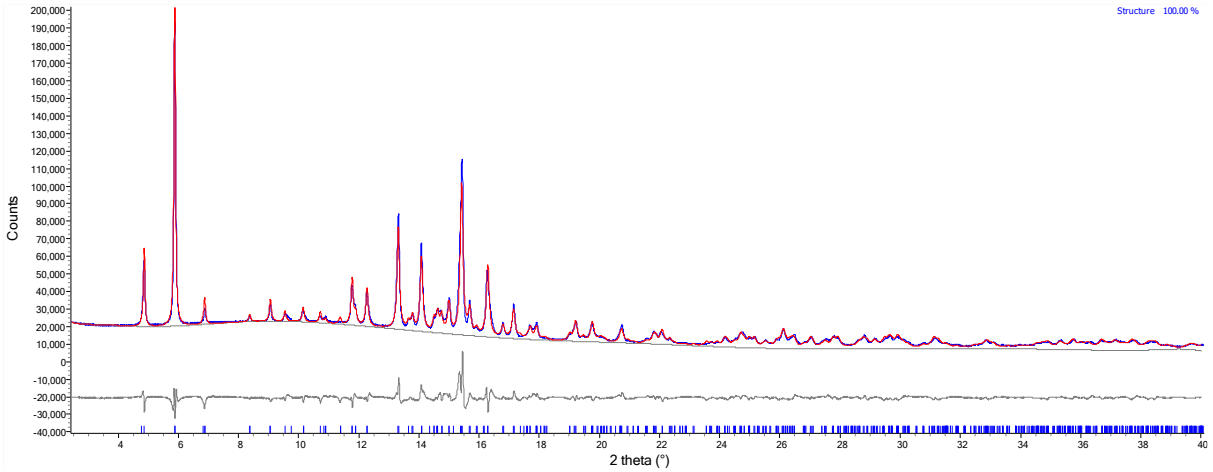

Figure S2.1. Rietveld fit for dehydrated $Cs_{6.2}$-MER.

Table S2.3. Refined structure of dehydrated $Cs_{6.2}$-MER.

Site	Type	x	y	z	Occ.	Mult.	B_{iso}
Cs1a	Cs	0	0	0.235(1)	0.80(1)	2	2
Cs2	Cs	-0.286(1)	0.5	0.277(1)	0.37(1)	4	2
Cs3	Cs	0	0.5	0.847(1)	0.64(1)	2	2
Cs31	Cs	0	0.5	0.390(1)	0.73(1)	2	2
O1	O	0.146(2)	-0.182(2)	0.068(3)	1	8	1
O2	O	0.180(2)	0.154(2)	0.434(3)	1	8	1
O3	O	-0.292(2)	-0.126(2)	0.224(3)	1	8	1
O4	O	-0.203(3)	0	0.062(4)	1	4	1
O5	O	-0.292(3)	0	0.430(4)	1	4	1
O6	O	-0.318(2)	0.134(2)	-0.042(3)	1	8	1
O7	O	0.130(2)	-0.322(2)	0.544(3)	1	8	1
O8	O	-0.114(2)	0.296(2)	0.276(3)	1	8	1
O9	O	0	-0.198(3)	0.444(4)	1	4	1
O10	O	0	-0.307(3)	0.060(4)	1	4	1
Si1	Si	0.283(1)	-0.119(1)	0.386(1)	0.81	8	1
Al1	Al	0.283(1)	-0.119(1)	0.386(1)	0.19	8	1
Si2	Si	-0.242(1)	-0.110(1)	0.081(1)	0.81	8	1
Al2	Al	-0.242(1)	-0.110(1)	0.081(1)	0.19	8	1
Si3	Si	0.389(1)	-0.207(1)	-0.117(1)	0.81	8	1
Al3	Al	0.389(1)	-0.207(1)	-0.117(1)	0.19	8	1
Si4	Si	0.395(1)	0.254(1)	0.577(2)	0.81	8	1
Al4	Al	0.395(1)	0.254(1)	0.577(2)	0.19	8	1

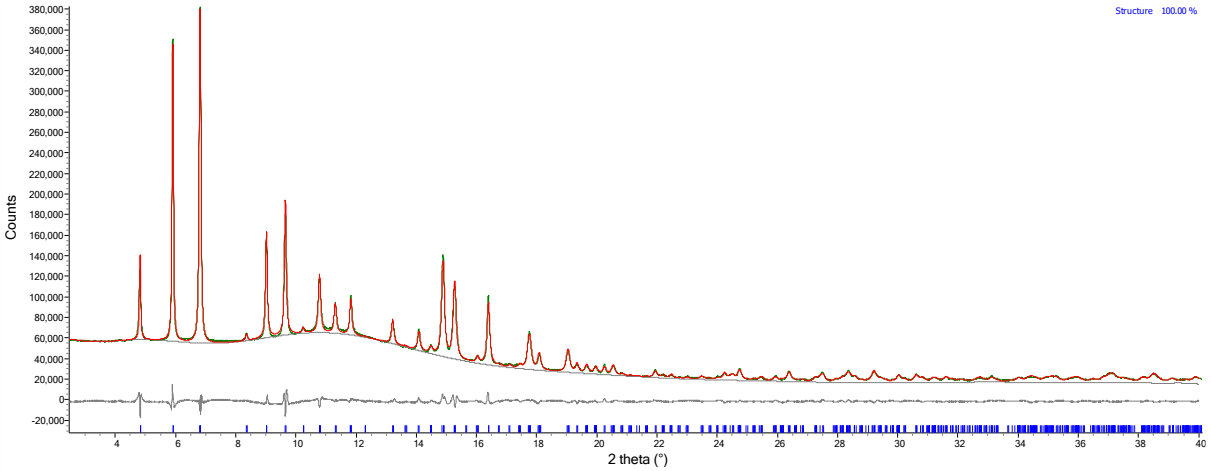

Figure S2.2. Rietveld fit for dehydrated $K_{6.2}$-MER.

Table S2.4. Refined structure of dehydrated $K_{6.2}$-MER.

Site	Type	x	y	z	Occ.	Mult.	B_{iso}
K1	K	0	0	0.497(2)	0.32(1)	2	2
K11	K	0	0	0.121(3)	0.30(1)	2	2
K2a	K	0.5	-0.208(1)	0.260(1)	0.59(1)	4	2
K2b	K	0.657(1)	0	0.790(1)	0.64(1)	4	2
O1	O	-0.176(1)	0.155(1)	0.068(2)	1	8	1
O2	O	0.157(1)	0.181(1)	0.433(2)	1	8	1
O3	O	-0.120(1)	-0.298(1)	0.230(3)	1	8	1
O4	O	0	-0.212(2)	0.058(3)	1	4	1
O5	O	0	-0.286(2)	0.440(3)	1	4	1
O6	O	0.140(1)	-0.328(1)	-0.031(2)	1	8	1
O7	O	-0.329(1)	0.134(1)	0.532(2)	1	8	1
O8	O	0.297(1)	-0.119(1)	0.271(2)	1	8	1
O9	O	-0.208(2)	0	0.443(2)	1	4	1
O10	O	-0.280(2)	0	0.059(2)	1	4	1
Si1	Si	-0.111(1)	0.291(1)	0.391(1)	0.81	8	1
Al1	Al	-0.111(1)	0.291(1)	0.391(1)	0.19	8	1
Si2	Si	-0.108(1)	-0.246(1)	0.085(1)	0.81	8	1
Al2	Al	-0.108(1)	-0.246(1)	0.085(1)	0.19	8	1
Si3	Si	-0.226(1)	0.386(1)	-0.108(1)	0.81	8	1
Al3	Al	-0.226(1)	0.386(1)	-0.108(1)	0.19	8	1
Si4	Si	0.251(1)	0.394(1)	0.578(1)	0.81	8	1
Al4	Al	0.251(1)	0.394(1)	0.578(1)	0.19	8	1

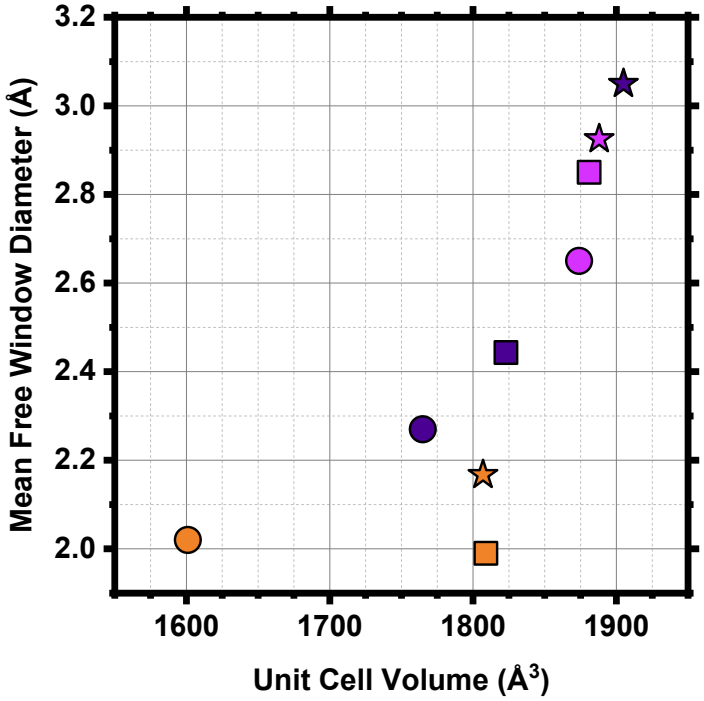

Figure S2.3. Comparison of pure cation forms of MER materials. Si/Al ratios of 2.3, 3.8 and 4.2 are indicated by circle, squares and stars, respectively. Na-, K- and Cs-forms are shown in orange, purple and pink, respectively. Data for lower silica materials are taken from Choi et al. and Georgieva et al.[1,8] $K_{1.2}Na_{5.0}$- data is shown in place of $Na_{6.2}$-MER due to unresolved symmetry.

S2.1.1. Alternative $K_{6.2}$-MER *P*4_2/*nmc* fit

Table S2.5. Crystallographic comparison of $K_{6.2}$-MER fitted with different space groups.

Sample	**$K_{6.2}$-MER**	**$K_{6.2}$-MER (alternative)**
Unit Cell	$K_{6.1}[Si_{25.8}Al_{6.2}O_{64}]$	$K_{6.0}[Si_{25.8}Al_{6.2}O_{64}]$
T (K)	298	298
Space Group	*Pmmn*	*P*4_2/*nmc*
X-ray Source	I11	I11
λ (Å)	0.826398	0.826398
***a* (Å)**	13.950(1)	13.919(1)
***b* (Å)**	13.894(1)	
***c* (Å)**	9.831(1)	9.831(1)
***V* (Å^3)**	1905(1)	1905(1)
R_{wp}	2.4	3.1
R_p	1.9	2.3
χ^2	24	37

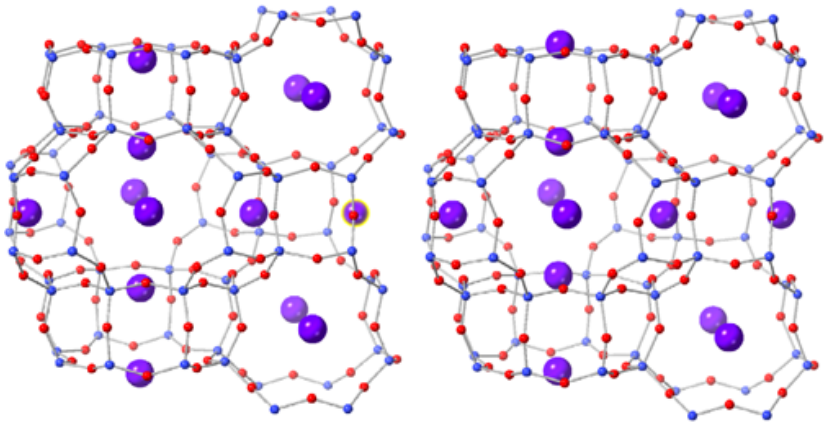

Figure S2.5. Comparison of crystal structures of $K_{6.2}$-MER fitted with (left) Pmmn and (right) $P4_2/nmc$. Note changes in cation positions in the d8r unit.

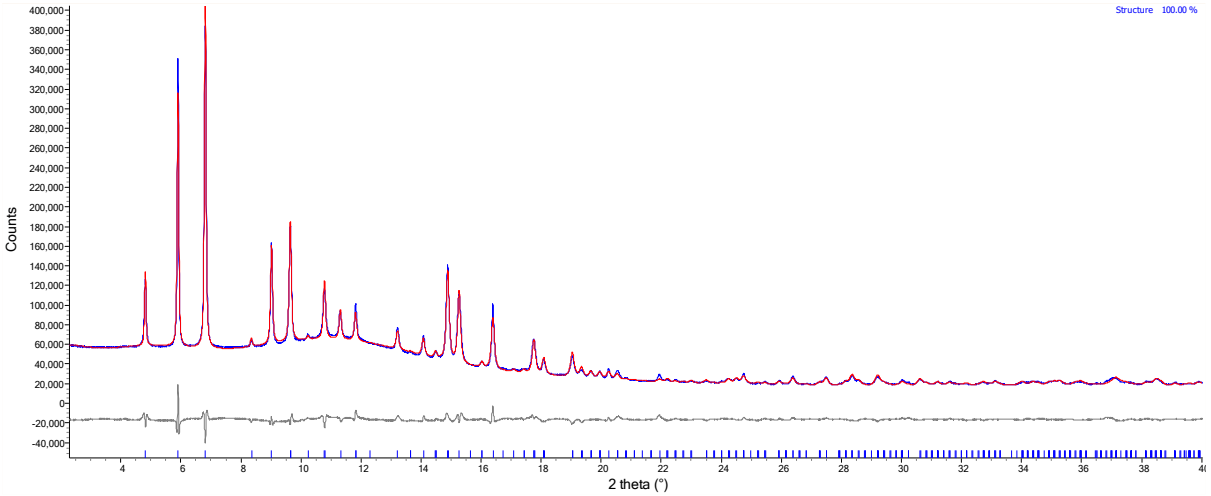

Figure S2.4. Rietveld fit for dehydrated $K_{6.2}$-MER in alternative space group, $P4_2/nmc$. Expt., blue; fit, red; difference, gray; tickmarks indicate peak positions.

Table S2.6. Refined structure of dehydrated $K_{6.2}$-MER in alternative space group, $P4_2/nmc$.

Site	Type	x	y	z	Occ.	Mult.	B_{iso}
K1	K	0	0	0.795(1)	0.30(1)	4	2
K2	K	0.181(1)	0.5	-0.025(1)	0.58(1)	8	2
O1	O	0.158(1)	0.178(1)	0.184(1)	1	16	1
O2	O	0.123(1)	0.295(1)	0	1	16	1
O3	O	0	0.287(1)	0.194(1)	1	8	1
O5	O	0.789(1)	0	0.184(1)	1	8	1
O4	O	0.171(1)	0.367(1)	0.229(1)	1	16	1
Si1	Si	0.111(1)	0.284(1)	0.147(1)	1	16	1
Al1	Al	0.111(1)	0.284(1)	0.147(1)	1	16	1
Si2	Si	0.752(1)	0.107(1)	0.163(1)	1	16	1
Al2	Al	0.752(1)	0.107(1)	0.163(1)	1	16	1

S2.2. Binary $K_{6.2-x}Na_x$-MER series data

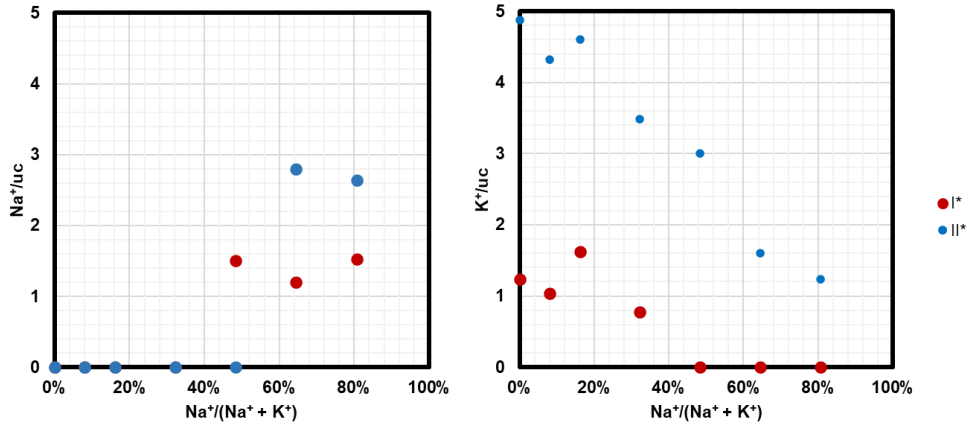

Figure S2.6. Cation siting in the $K_{6.2-x}Na_x$-MER series. Absolute cations/uc are shown for sites I (red) and II* (blue) for Na^+ (left) and K^+ (right) with varying Na^+ content.*

Table S2.7. Crystallography of $K_{6.2-x}Na_x$-MER materials in this work.

Sample	**$K_{5.7}Na_{0.5}$-MER**	**$K_{5.2}Na_{1.0}$-MER**	**$K_{4.2}Na_{1.0}$-MER**
Unit Cell	$K_{5.4}[Si_{25.8}Al_{6.2}O_{64}]$	$K_{6.1}[Si_{25.8}Al_{6.2}O_{64}]$	$K_{4.3}[Si_{25.8}Al_{6.2}O_{64}]$
T (K)	298	298	298
Space Group	*Pmmn*	*Pmmn*	*Pmmn*
X-ray Source	I11	Stoe	Stoe
λ (Å)	0.826398	1.54060	1.54060
***a* (Å)**	13.978(1)	13.918(1)	13.753(1)
***b* (Å)**	13.913(1)	13.746(1)	13.647(1)
***c* (Å)**	9.820(1)	9.862(1)	9.851(1)
***V* (Å^3)**	1910(1)	1887(1)	1849(1)
R_{wp}	3.3	6.1	5.7
R_p	2.4	4.7	4.5
χ^2	48	8	5
Sample	**$K_{3.2}Na_{3.0}$-MER**	**$K_{2.2}Na_{4.0}$-MER**	**$K_{1.2}Na_{5.0}$-MER**
Unit Cell	$K_{3.0}Na_{1.5}[Si_{25.8}Al_{6.2}O_{64}]$	$K_{1.5}Na_{4.1}[Si_{25.8}Al_{6.2}O_{64}]$	$K_{1.2}Na_{4.2}[Si_{25.8}Al_{6.2}O_{64}]$
T (K)	298	298	298
Space Group	*Pmmn*	*Pmmn*	*Pmmn*
X-ray Source	I11	Stoe	I11
λ (Å)	0.826398	1.54060	0.826398
***a* (Å)**	13.671(1)	13.629(1)	13.606(1)
***b* (Å)**	13.598(1)	13.564(1)	13.551(1)
***c* (Å)**	9.864(1)	9.846(1)	9.845(1)
***V* (Å^3)**	1833(1)	1820(1)	1815(1)
R_{wp}	3.3	5.8	3.4
R_p	2.4	4.5	2.4
χ^2	48	7	47

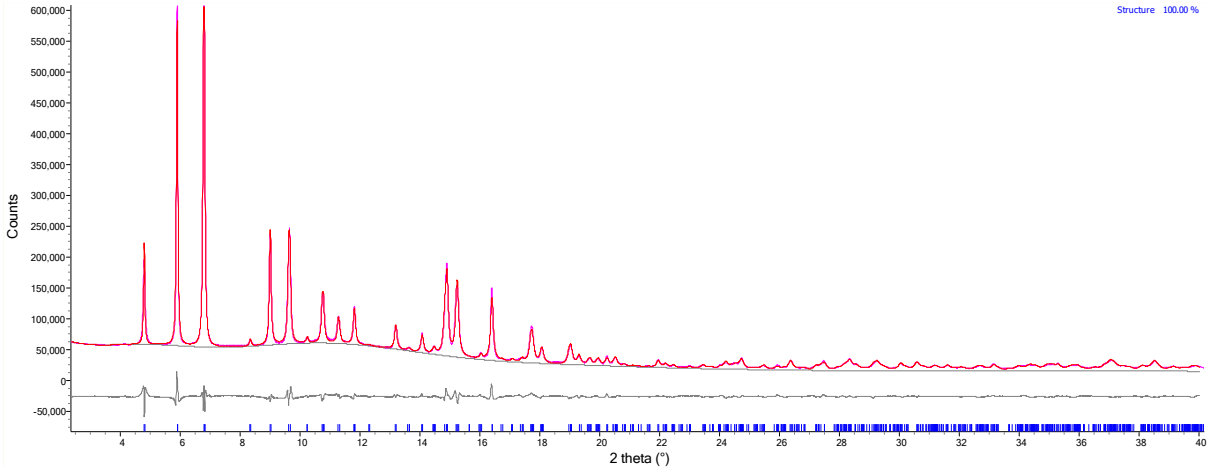

Figure S2.7. Rietveld fit for dehydrated $K_{5.7}Na_{0.5}$-MER.

Table S2.8. Refined structure of dehydrated $K_{5.7}Na_{0.5}$-MER.

Site	Type	x	y	z	Occ.	Mult.	B_{iso}
K1	K	0	0	0.494(3)	0.22(1)	2	2
K11	K	0	0	0.129(2)	0.30(1)	2	2
K2a	K	0.5	-0.199(1)	0.250(1)	0.47(1)	4	2
K2b	K	0.656(1)	0	0.788(1)	0.61(1)	4	2
O1	O	-0.175(1)	0.158(1)	0.068(2)	1	8	1
O2	O	0.157(1)	0.182(1)	0.431(2)	1	8	1
O3	O	-0.118(1)	-0.297(1)	0.229(2)	1	8	1
O4	O	0	-0.216(1)	0.053(2)	1	4	1
O5	O	0	-0.287(1)	0.444(2)	1	4	1
O6	O	0.137(1)	-0.333(1)	-0.028(2)	1	8	1
O7	O	-0.331(1)	0.132(1)	0.531(2)	1	8	1
O8	O	0.301(1)	-0.119(1)	0.270(2)	1	8	1
O9	O	-0.206(1)	0	0.439(2)	1	4	1
O10	O	-0.276(1)	0	0.056(2)	1	4	1
Si1	Si	-0.109(1)	0.292(1)	0.395(1)	0.81	8	1
Al1	Al	-0.109(1)	0.292(1)	0.395(1)	0.19	8	1
Si2	Si	-0.108(1)	-0.247(1)	0.082(1)	0.81	8	1
Al2	Al	-0.108(1)	-0.247(1)	0.082(1)	0.19	8	1
Si3	Si	-0.228(1)	0.384(1)	-0.105(1)	0.81	8	1
Al3	Al	-0.228(1)	0.384(1)	-0.105(1)	0.19	8	1
Si4	Si	0.251(1)	0.393(1)	0.578(1)	0.81	8	1
Al4	Al	0.251(1)	0.393(1)	0.578(1)	0.19	8	1

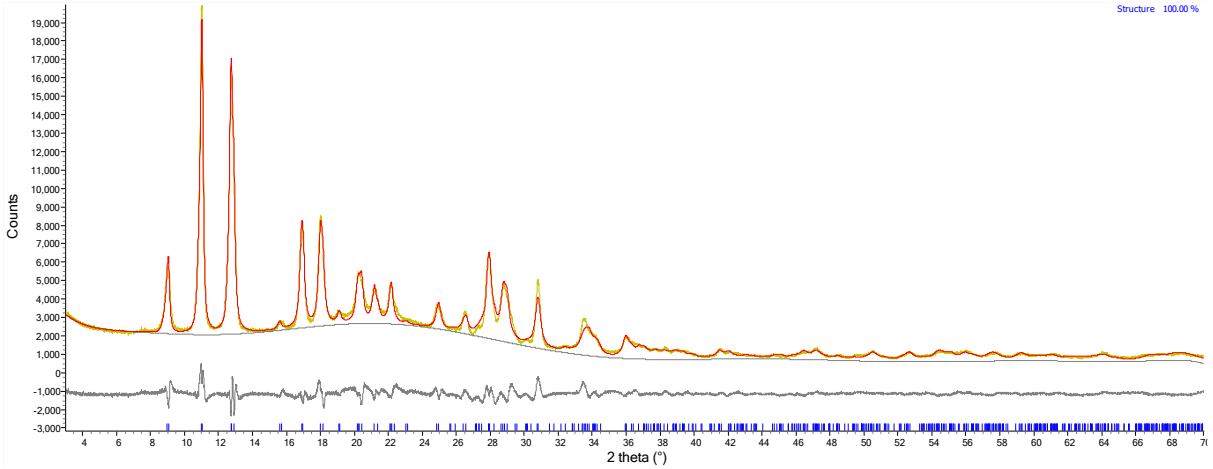

Figure S2.8. Rietveld fit for dehydrated $K_{5.2}Na_{1.0}$-MER.

Table S2.9. Refined structure of dehydrated $K_{5.2}Na_{1.0}$-MER.

Site	Type	x	y	z	Occ.	Mult.	B_{iso}
K11	K	0	0	0.014(2)	0.81(2)	2	2
K2a	K	0.5	-0.183(3)	0.153(4)	0.37(2)	4	2
K2b	K	0.680(1)	0	0.780(2)	0.78(1)	4	2
O1	O	-0.180(2)	0.170(2)	0.070(3)	1	8	1
O2	O	0.145(2)	0.184(2)	0.421(3)	1	8	1
O3	O	-0.112(2)	-0.317(2)	0.232(3)	1	8	1
O4	O	0	-0.211(2)	0.074(4)	1	4	1
O5	O	0	-0.305(3)	0.446(4)	1	4	1
O6	O	0.129(2)	-0.339(2)	-0.027(3)	1	8	1
O7	O	-0.317(2)	0.133(3)	0.527(3)	1	8	1
O8	O	0.289(2)	-0.123(2)	0.266(3)	1	8	1
O9	O	-0.195(3)	0	0.428(5)	1	4	1
O10	O	-0.277(3)	0	0.060(4)	1	4	1
Si1	Si	-0.110(1)	0.291(1)	0.394(2)	1	8	1
Al1	Al	-0.110(1)	0.291(1)	0.394(2)	0.19	8	1
Si2	Si	-0.113(1)	-0.260(1)	0.090(2)	0.81	8	1
Al2	Al	-0.113(1)	-0.260(1)	0.090(2)	0.19	8	1
Si3	Si	-0.227(1)	0.384(1)	-0.092(2)	0.81	8	1
Al3	Al	-0.227(1)	0.384(1)	-0.092(2)	0.19	8	1
Si4	Si	0.273(1)	0.390(1)	0.592(2)	0.81	8	1
Al4	Al	0.273(1)	0.390(1)	0.592(2)	0.19	8	1

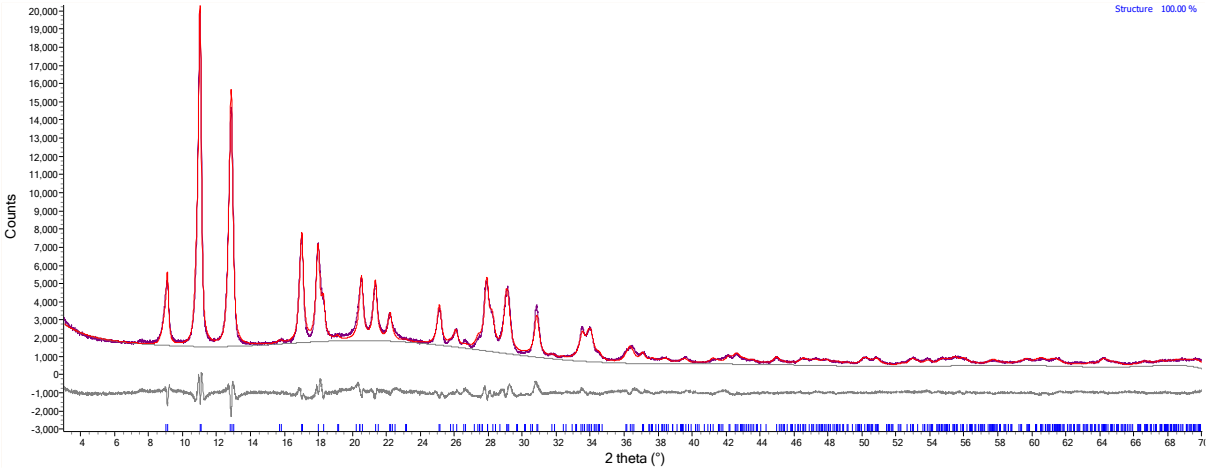

Figure S2.9. Rietveld fit for dehydrated $K_{4.2}Na_{2.0}$-MER.

Table S2.10. Refined structure of dehydrated $K_{4.2}Na_{2.0}$-MER.

Site	Type	x	y	z	Occ.	Mult.	B_{iso}
K11	K	0	0	0.100(3)	0.39(1)	2	2
K2a	K	0.5	-0.068(1)	0.185(2)	0.41(1)	4	2
K2b	K	0.711(1)	0	0.732(4)	0.46(1)	4	2
O1	O	0	0.195(2)	0.060(3)	1	8	1
O2	O	0.132(2)	0.181(2)	0.420(3)	1	8	1
O3	O	-0.111(1)	-0.329(1)	0.246(4)	1	8	1
O4	O	0	-0.310(3)	0.025(4)	1	4	1
O5	O	0	-0.318(3)	0.466(4)	1	4	1
O6	O	0.178(2)	-0.383(2)	0.006(3)	1	8	1
O7	O	-0.311(2)	0.145(2)	0.509(3)	1	8	1
O8	O	0.269(1)	-0.121(1)	0.250(4)	1	8	1
O9	O	-0.198(3)	0	0.432(5)	1	4	1
O10	O	-0.180(3)	0	0.085(5)	1	4	1
Si1	Si	-0.108(1)	0.293(1)	0.406(2)	1	8	1
Al1	Al	-0.108(1)	0.293(1)	0.406(2)	0.19	8	1
Si2	Si	-0.112(1)	-0.303(1)	0.083(2)	0.81	8	1
Al2	Al	-0.112(1)	-0.303(1)	0.083(2)	0.19	8	1
Si3	Si	-0.271(2)	0.390(1)	-0.091(2)	0.81	8	1
Al3	Al	-0.271(2)	0.390(1)	-0.091(2)	0.19	8	1
Si4	Si	0.275(2)	0.390(1)	0.593(2)	0.81	8	1
Al4	Al	0.275(2)	0.390(1)	0.593(2)	0.19	8	1

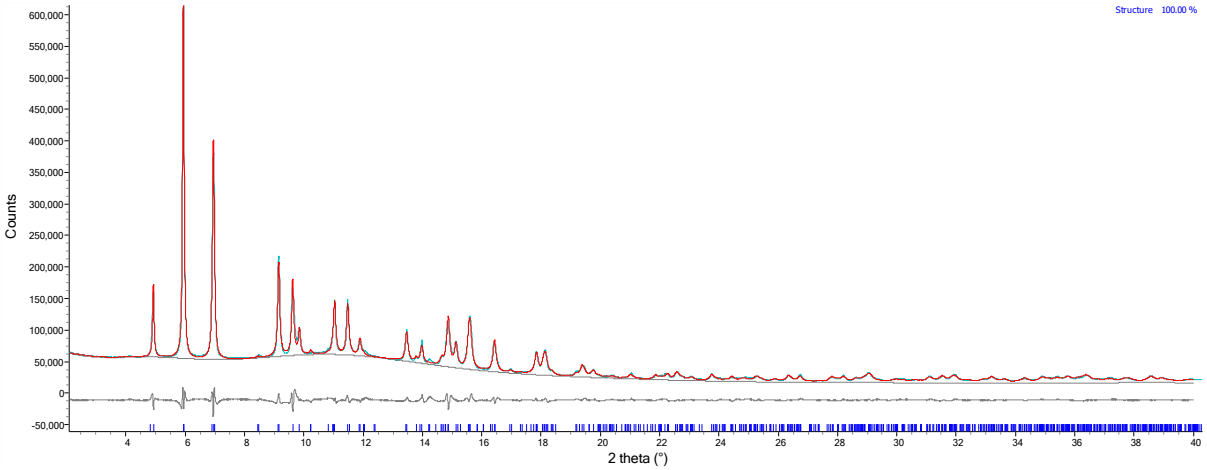

Figure S2.10. Rietveld fit for dehydrated $K_{3.2}Na_{3.0}$-MER.

Table S2.11. Refined structure of dehydrated $K_{3.2}Na_{3.0}$-MER.

Site	Type	x	y	z	Occ.	Mult.	B_{iso}
Na1	Na	0	0	0.445(3)	0.45(2)	2	2
Na11	Na	0	0	0.201(4)	0.30(1)	2	2
K2a	K	-0.209(1)	0.5	0.207(2)	0.37(1)	4	2
K2b	K	0	0.559(1)	0.690(2)	0.38(1)	4	2
O1	O	0.135(1)	-0.187(2)	0.071(2)	1	8	1
O2	O	0.144(1)	0.191(2)	0.427(2)	1	8	1
O3	O	-0.270(1)	-0.122(1)	0.240(2)	1	8	1
O4	O	-0.182(2)	0	0.060(2)	1	4	1
O5	O	-0.186(1)	0	0.404(2)	1	4	1
O6	O	-0.311(1)	0.133(2)	-0.014(2)	1	8	1
O7	O	0.185(1)	-0.376(2)	0.492(2)	1	8	1
O8	O	-0.118(1)	0.333(1)	0.257(2)	1	8	1
O9	O	0	-0.317(2)	0.470(2)	1	4	1
O10	O	0	-0.321(2)	0.033(2)	1	4	1
Si1	Si	0.234(1)	-0.114(1)	0.399(1)	0.81	8	1
Al1	Al	0.234(1)	-0.114(1)	0.399(1)	0.19	8	1
Si2	Si	-0.219(1)	-0.106(1)	0.088(1)	0.81	8	1
Al2	Al	-0.219(1)	-0.106(1)	0.088(1)	0.19	8	1
Si3	Si	0.391(1)	-0.206(1)	-0.102(1)	0.81	8	1
Al3	Al	0.391(1)	-0.206(1)	-0.102(1)	0.19	8	1
Si4	Si	0.390(1)	0.189(1)	0.577(1)	0.81	8	1
Al4	Al	0.390(1)	0.189(1)	0.577(1)	0.19	8	1

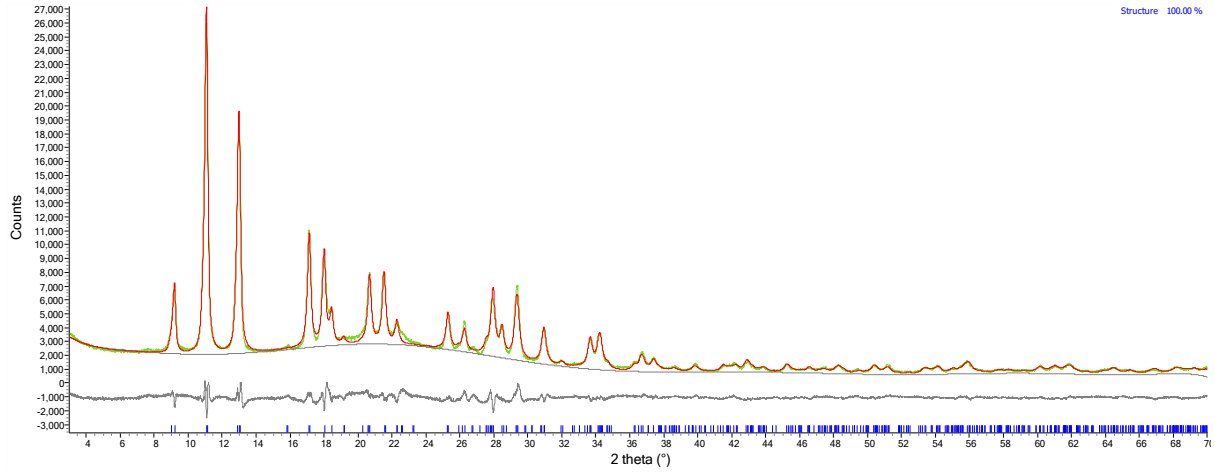

Figure S2.11. Rietveld fit for dehydrated $K_{2.2}Na_{4.0}$-MER.

Table S2.12. Refined structure of dehydrated $K_{2.2}Na_{4.0}$-MER.

Site	Type	x	y	z	Occ.	Mult.	B_{iso}
Na11	Na	0	0	0.081(3)	0.60(2)	2	2
K2b	K	0.5	-0.062(1)	0.189(2)	0.37(1)	4	2
Na2a	Na	0.707(1)	0	0.718(3)	0.73(2)	4	2
O1	O	-0.150(2)	0.196(2)	0.062(3)	1	8	1
O2	O	0.130(2)	0.187(2)	0.422(3)	1	8	1
O3	O	-0.111(1)	-0.333(1)	0.243(3)	1	8	1
O4	O	0	-0.319(3)	0.021(4)	1	4	1
O5	O	0	-0.330(3)	0.463(4)	1	4	1
O6	O	0.182(2)	-0.385(2)	0.005(3)	1	8	1
O7	O	-0.308(2)	0.137(2)	0.514(3)	1	8	1
O8	O	0.262(1)	-0.115(1)	0.253(3)	1	8	1
O9	O	-0.183(3)	0	0.437(4)	1	4	1
O10	O	-0.171(3)	0	0.084(4)	1	4	1
Si1	Si	-0.109(1)	0.298(1)	0.398(2)	1	8	1
Al1	Al	-0.109(1)	0.298(1)	0.398(2)	0.19	8	1
Si2	Si	-0.113(1)	-0.309(1)	0.081(2)	0.81	8	1
Al2	Al	-0.113(1)	-0.309(1)	0.081(2)	0.19	8	1
Si3	Si	-0.272(1)	0.390(1)	-0.096(2)	0.81	8	1
Al3	Al	-0.272(1)	0.390(1)	-0.096(2)	0.19	8	1
Si4	Si	0.280(1)	0.389(1)	0.588(2)	0.81	8	1
Al4	Al	0.280(1)	0.389(1)	0.588(2)	0.19	8	1

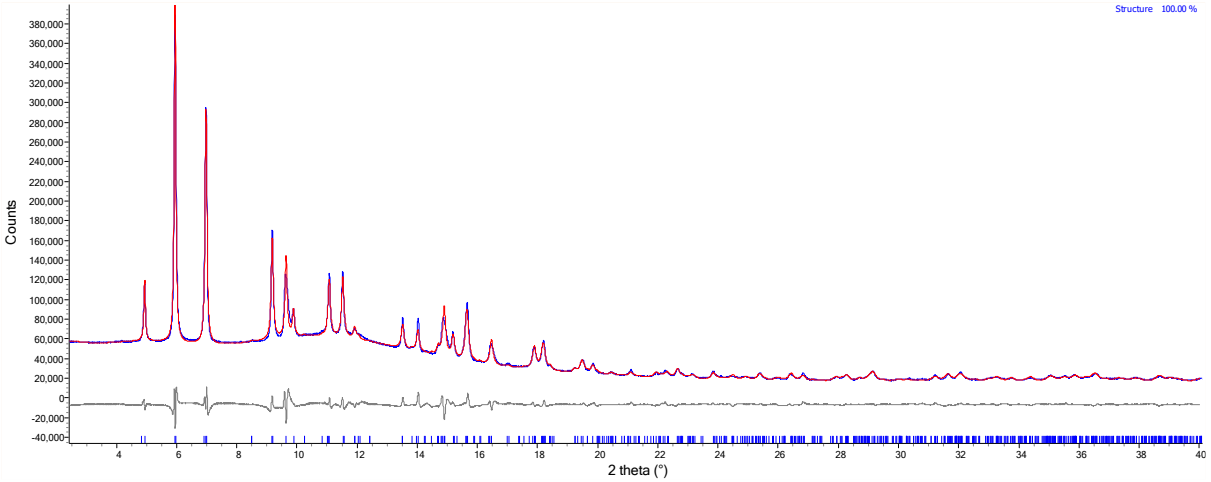

Figure S2.12. Rietveld fit for dehydrated $K_{1.2}Na_{5.0}$-MER.

Table S2.13. Refined structure of dehydrated $K_{1.2}Na_{5.0}$-MER.

Site	Type	x	y	z	Occ.	Mult.	B_{iso}
Na11	Na	0	0	-0.040(2)	0.09(3)	2	2
Na1	Na	0	0	0.445(3)	0.67(3)	2	2
K2a	K	0.5	-0.070(1)	0.189(3)	0.31(1)	4	2
Na2b	Na	0.706(1)	0	0.704(2)	0.66(2)	4	2
O1	O	0.134(2)	-0.190(2)	0.068(3)	1	8	1
O2	O	0.141(2)	0.189(2)	0.422(3)	1	8	1
O3	O	-0.263(1)	-0.118(1)	0.239(3)	1	8	1
O4	O	-0.174(3)	0	0.061(4)	1	4	1
O5	O	-0.184(3)	0	0.418(4)	1	4	1
O6	O	-0.307(2)	0.124(2)	-0.018(2)	1	8	1
O7	O	0.185(2)	-0.372(2)	0.497(3)	1	8	1
O8	O	-0.117(1)	0.335(1)	0.246(3)	1	8	1
O9	O	0	-0.319(3)	0.470(3)	1	4	1
O10	O	0	-0.332(3)	0.025(3)	1	4	1
Si1	Si	0.231(1)	-0.107(1)	0.391(1)	0.81	8	1
Al1	Al	0.231(1)	-0.107(1)	0.391(1)	0.19	8	1
Si2	Si	-0.219(1)	-0.111(1)	0.090(1)	0.81	8	1
Al2	Al	-0.219(1)	-0.111(1)	0.090(1)	0.19	8	1
Si3	Si	0.386(2)	-0.196(1)	-0.076(1)	0.81	8	1
Al3	Al	0.386(2)	-0.196(1)	-0.076(1)	0.19	8	1
Si4	Si	0.386(2)	0.193(1)	0.602(1)	0.81	8	1
Al4	Al	0.386(2)	0.193(1)	0.602(1)	0.19	8	1

S3. Adsorption studies

S3.1. Ar adsorption

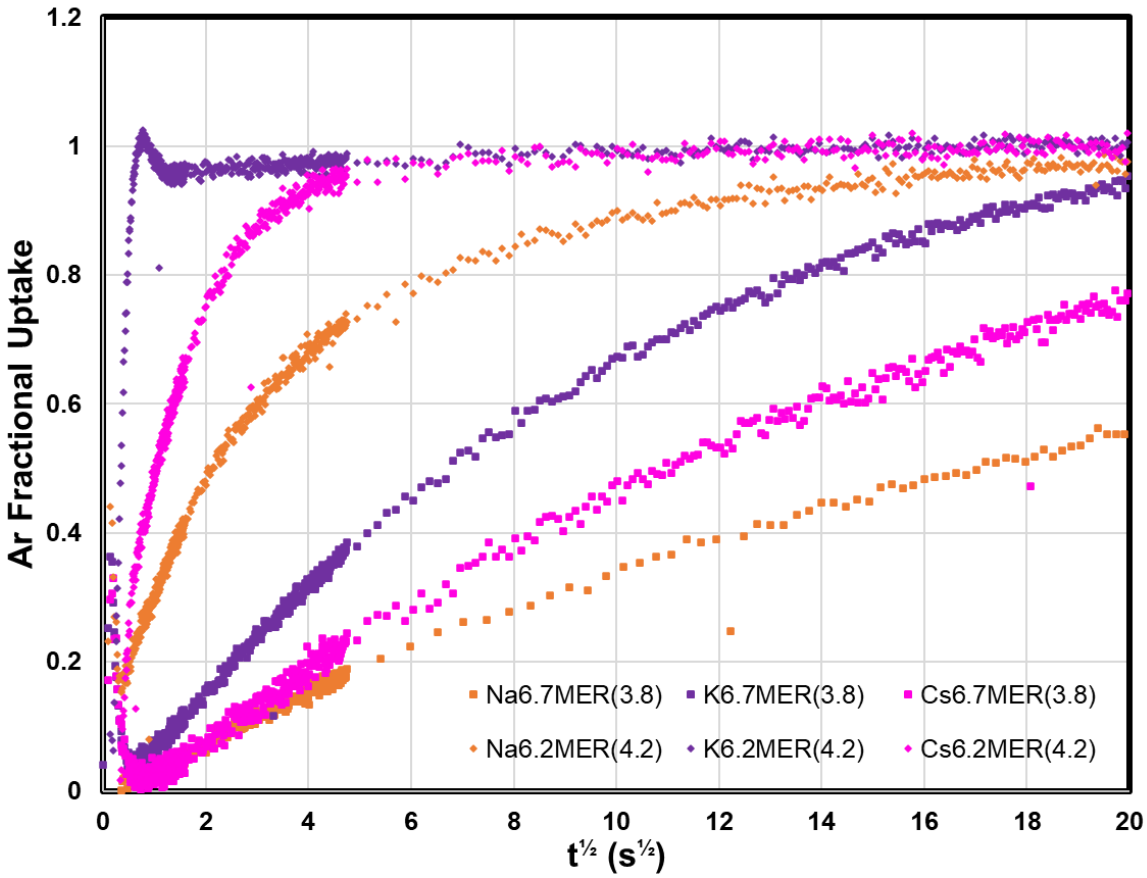

Figure S3.1. Fractional Ar adsorption uptake curves of MER materials. Na-, K- and Cs-forms are shown in orange, purple and pink with Si/Al = 3.8 and 4.2 indicated by squares and diamonds, respectively.

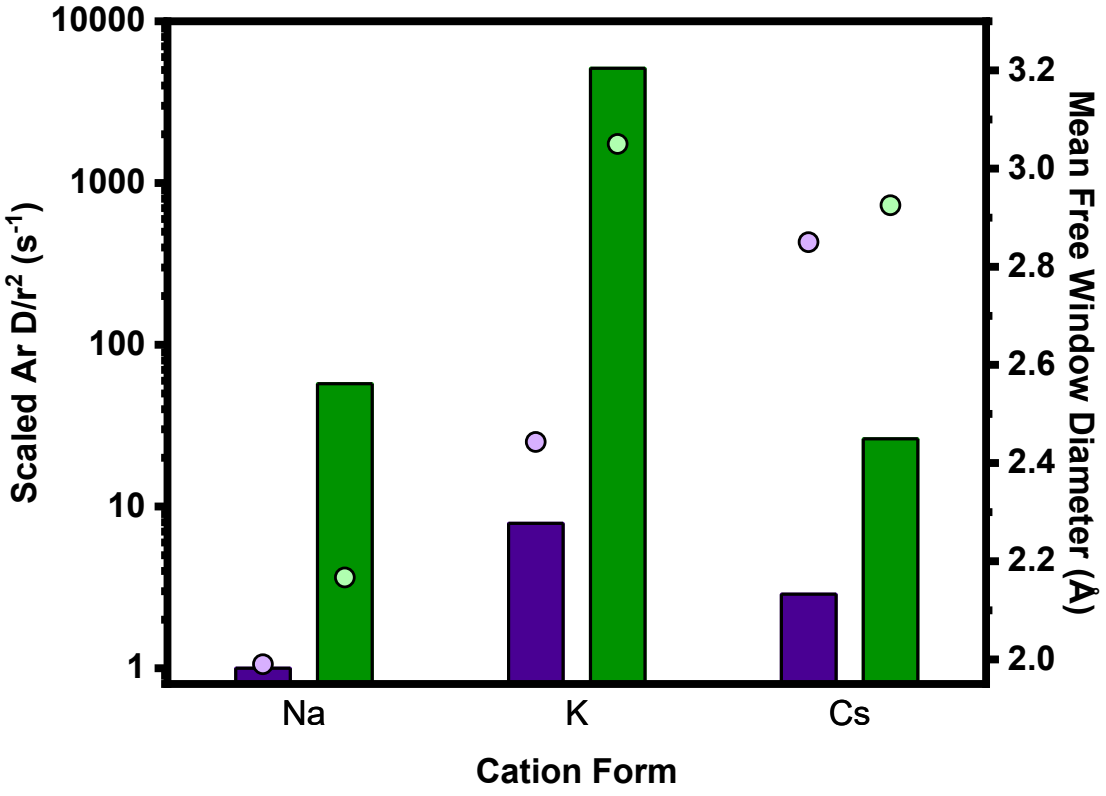

Figure S3.2. Ar uptake rates at 800 mbar (bars) and mean free window diameter (points). Data relating to the Si/Al = 3.8 and 4.2 are shown in purple and green, respectively. Diffusivities are scaled relative to the smallest value ($Na_{6.7}$-MER, $8x10^{-5}$ s^{-1}). $K_{1.2}Na_{5.0}$-MER (4.2) data has been used in place of $Na_{6.2}$-MER.

S3.2. CO_2 adsorption

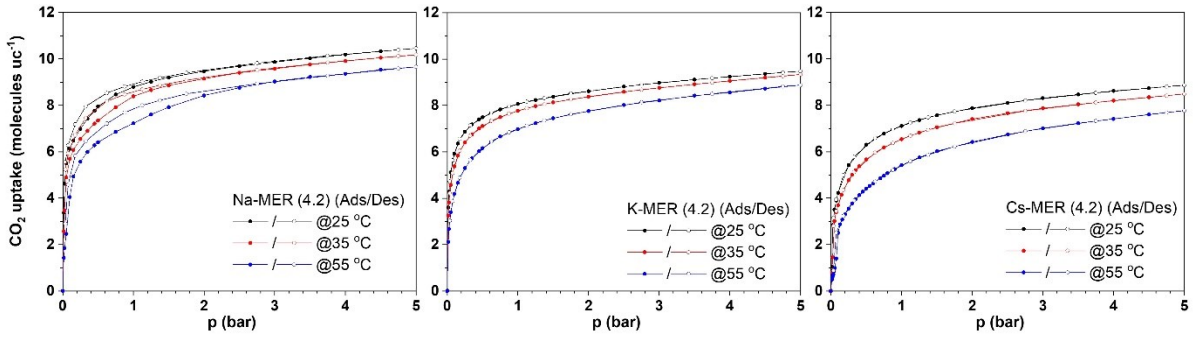

Figure S3.3. CO_2 sorption isotherms at 298 K for $Na_{6.2}$-, $K_{6.2}$- and $Cs_{6.2}$-MER up to 5 bar, scaled to CO_2 molecules/uc. Adsorption and desorption branches are shown closed and open symbols, respectively.

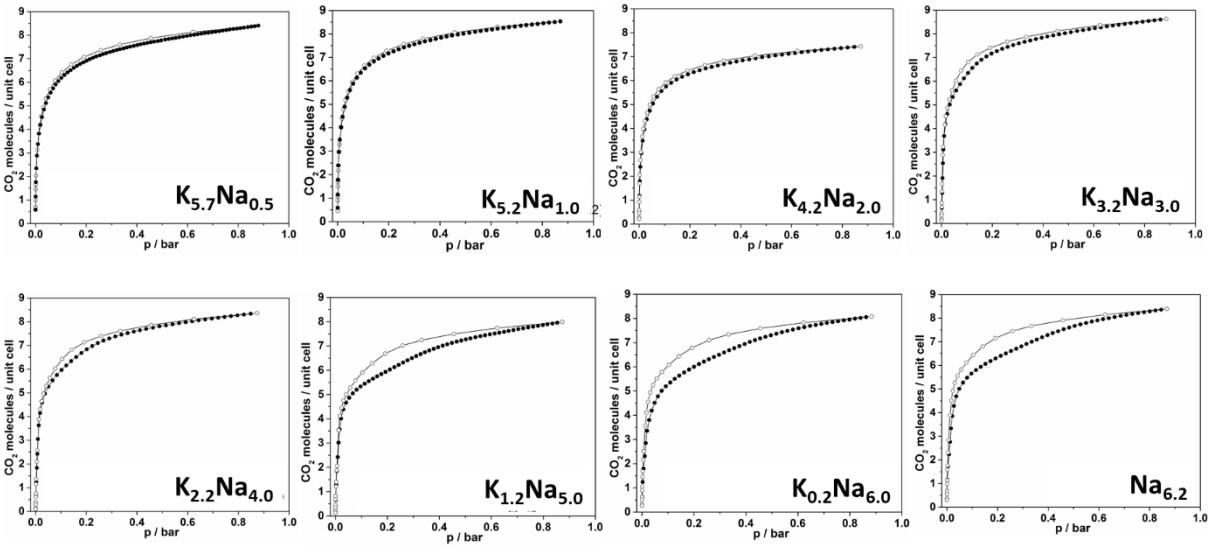

Figure S3.4. CO_2 sorption isotherms at 298 K of the $K_{6.2-x}Na_x$-MER series, with adsorption and desorption branches shown by closed and open circles, respectively.

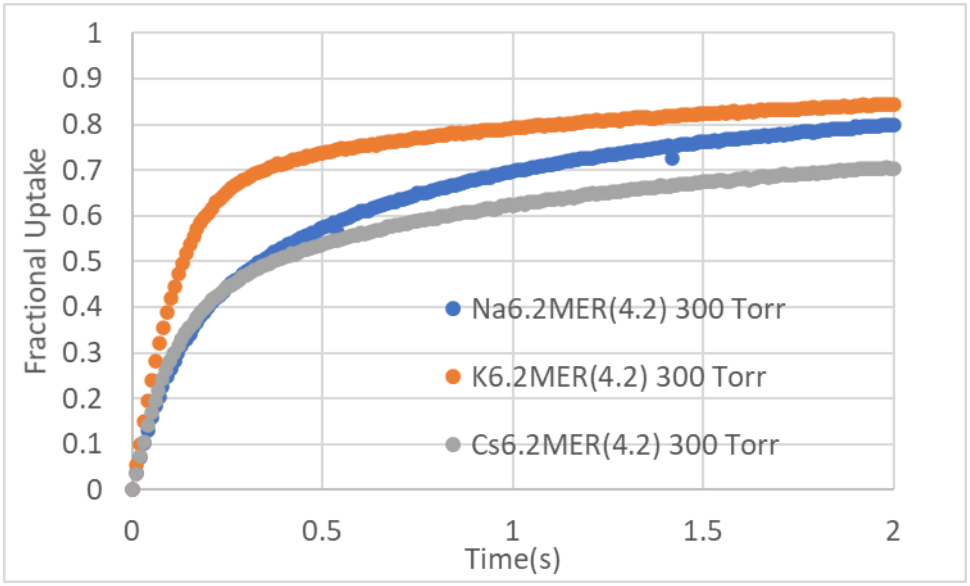

Figure S3.5. Fractional CO_2 uptake curves at 300 Torr.

S4. Comparison of $Na_{6.2}$- and $Na_{5.0}K_{1.2}$-MER

Due to the challenging nature of the structure of $Na_{6.2}$-MER, it was necessary to use $Na_{5.0}K_{1.2}$-MER as a Na-form of MER (4.2) when examining the effect of varying Si/Al in MER materials. We believe that this is a valid approach due to the similarity in unit cell and CO_2 isotherm.

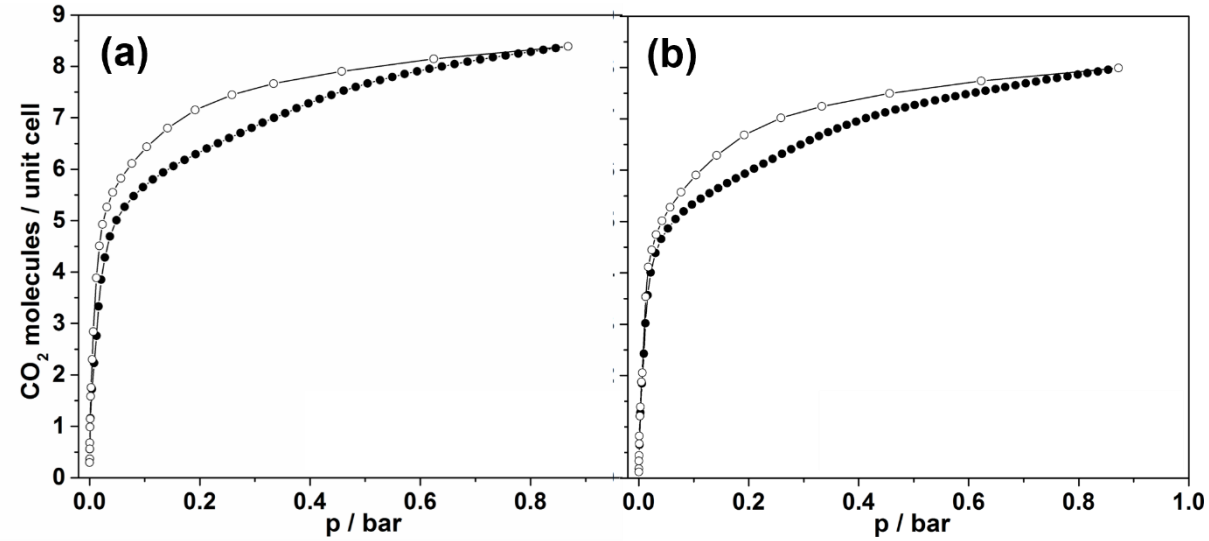

Figure S4.1. CO_2 sorption isotherms of (a) $Na_{6.2}$- and (b) $Na_{5.0}K_{1.2}$-MER. Adsorption and desorption branches are shown as closed and open circles, respectively.

S5. Crystallographic details of the refined dehydrated solids with adsorbed CO_2

S5.1. $Cs_{6.2}$-MER

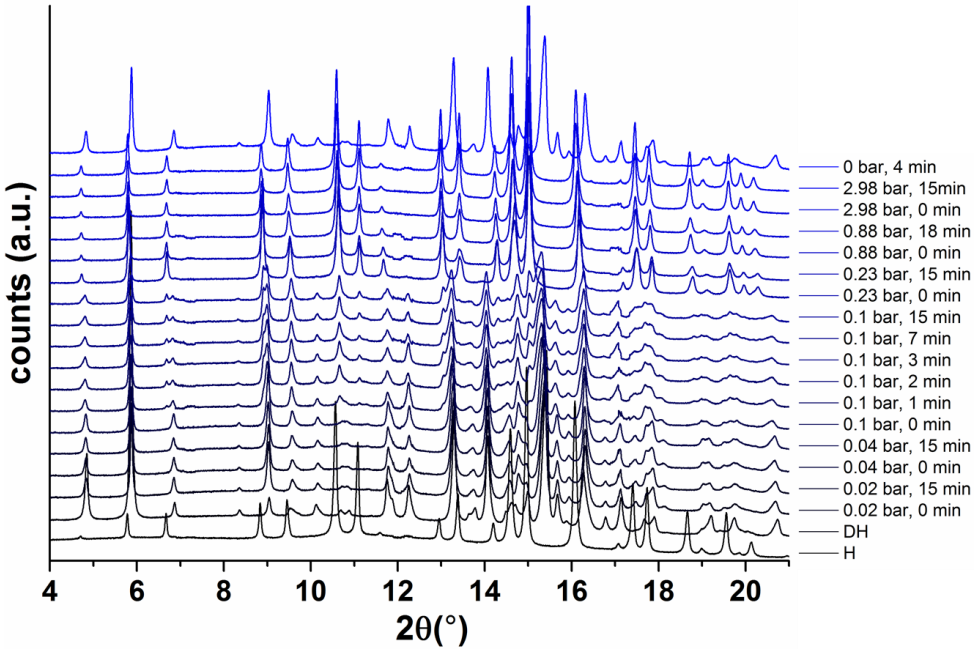

Figure S5.1. Synchrotron in situ VPXRD data for $Cs_{6.2}$-MER.

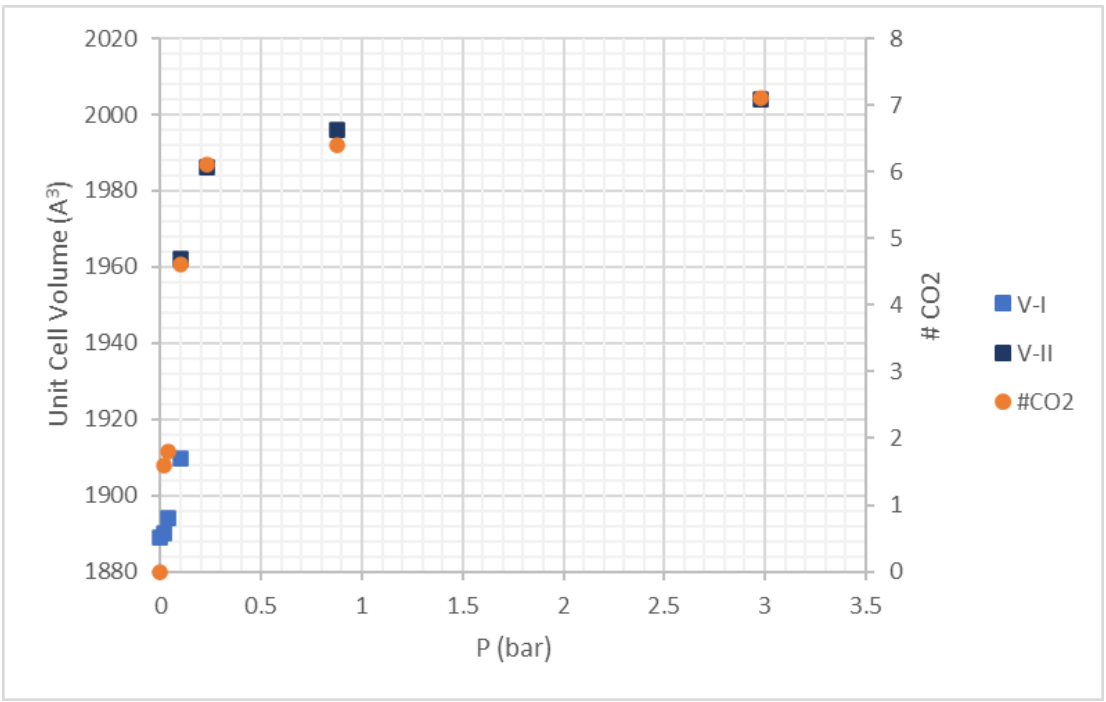

Figure S5.2. Unit cell volume and CO_2 content (molecules uc^{-1}) data from $Cs_{6.2}$-MER refinements with pressure. V-I and V-II correspond to narrow- and wide-pore forms, respectively.

Table S5.1. Crystallography of $Cs_{6.2}$-MER under CO_2 exposure.

Sample	**$Cs_{6.2}$-MER (dh)**	**$Cs_{6.2}$-MER (20 mbar)**	**$Cs_{6.2}$-MER (40 mbar)**
Unit Cell	$Cs_{5.9}[Si_{25.8}Al_{6.2}O_{64}]$	$Cs_{5.5}[Si_{25.8}Al_{6.2}O_{64}]$ $.(CO_2)_{1.6}$	$Cs_{5.5}[Si_{25.8}Al_{6.2}O_{64}]$ $.(CO_2)_{1.8}$
T (K)	298	298	298
Space Group	*Pmmn*	*P4$_2$/nmc*	*P4$_2$/nmc*
X-ray Source	I11	I11	I11
λ (Å)	0.826398	0.826398	0.826398
***a* (Å)**	13.794(1)	13.819(1)	13.833(1)
***b* (Å)**	13.776(1)		
***c* (Å)**	9.940(1)	9.897(1)	9.898(1)
***V* (Å^3)**	1889(1)	1890(1)	1894(1)
***R*$_{wp}$**	5.5	5.5	5.5
***R*$_p$**	3.8	3.7	3.7
χ^2	54	53	53

Sample	**$Cs_{6.2}$-MER (100 mbar, narrow)**	**$Cs_{6.2}$-MER (100 mbar, wide)**
Unit Cell	$Cs_{5.5}[Si_{25.8}Al_{6.2}O_{64}].(CO_2)_{2.0}$	$Cs_{4.8}[Si_{25.8}Al_{6.2}O_{64}].(CO_2)_{7.7}$
T (K)	298	298
Space Group	*P4$_2$/nmc*	*P4$_2$/nmc*
X-ray Source	I11	
λ (Å)	0.826398	0.826398
***a* (Å)**	13.874(1)	14.077(1)
***c* (Å)**	9.921(1)	9.903(1)
***V* (Å^3)**	1910(1)	1962(1)
***R*$_{wp}$**	4.8	
***R*$_p$**	3.3	
χ^2	38	

Sample	**$Cs_{6.2}$-MER (230 mbar)**	**$Cs_{6.2}$-MER (880 mbar)**	**$Cs_{6.2}$-MER (2980 mbar)**
Unit Cell	$Cs_{4.8}[Si_{25.8}Al_{6.2}O_{64}]$ $.(CO_2)_{6.1}$	$Cs_{5.3}[Si_{25.8}Al_{6.2}O_{64}]$ $.(CO_2)_{6.4}$	$Cs_{5.8}[Si_{25.8}Al_{6.2}O_{64}]$ $.(CO_2)_{7.1}$
T (K)	298	298	298
Space Group	*P4$_2$/nmc*	*P4$_2$/nmc*	*P4$_2$/nmc*
X-ray Source	I11	I11	I11
λ (Å)	0.826398	0.826398	0.826398
***a* (Å)**	14.129(1)	14.143(1)	14.152(1)
***c* (Å)**	9.949(1)	9.978(1)	10.007(1)
***V* (Å^3)**	1986(1)	1996(1)	2004(1)
***R*$_{wp}$**	4.2	3.3	4.3
***R*$_p$**	2.8	2.2	2.9
χ^2	27	17	32

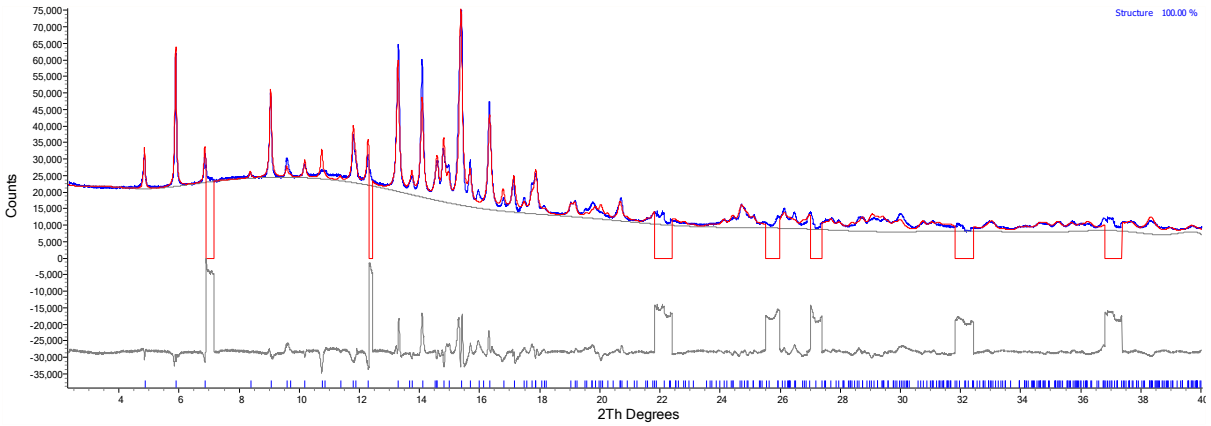

Figure S5.3. Rietveld fit for $Cs_{6.2}$-MER at 20 mbar. Note sections are cut out due to background effects.

Table S5.2. Refined structure of $Cs_{6.2}$-MER at 20 mbar.

Site	Type	x	y	z	Occ.	Mult.	B_{iso}
Cs1a	Cs	0	0	0	0.48(1)	2	2
Cs2	Cs	0.5	0.695(1)	0	0.30(1)	8	2
Cs3	Cs	0	0.5	0.119(1)	0.58(1)	4	2
O1	O	0.177(1)	0.150(1)	0.191(1)	1	16	1
O2	O	0.129(1)	0.299(1)	0	1	16	1
O3	O	0	0.202(1)	0.174(2)	1	8	1
O5	O	0.705(1)	0.000	0.198(2)	1	8	1
O4	O	0.129(1)	0.318(1)	0.280(1)	1	16	1
Si1	Si	0.107(1)	0.243(1)	0.152(1)	0.81	16	1
Al1	Al	0.107(1)	0.243(1)	0.152(1)	0.19	16	1
Si2	Si	0.713(1)	0.115(1)	0.150(1)	0.81	16	1
Al2	Al	0.713(1)	0.115(1)	0.150(1)	0.19	16	1
C1	C	0.5	0.5	0	0.81(1)	2	4
OC1	O	0.5	0.5	0.117	0.81(1)	4	4

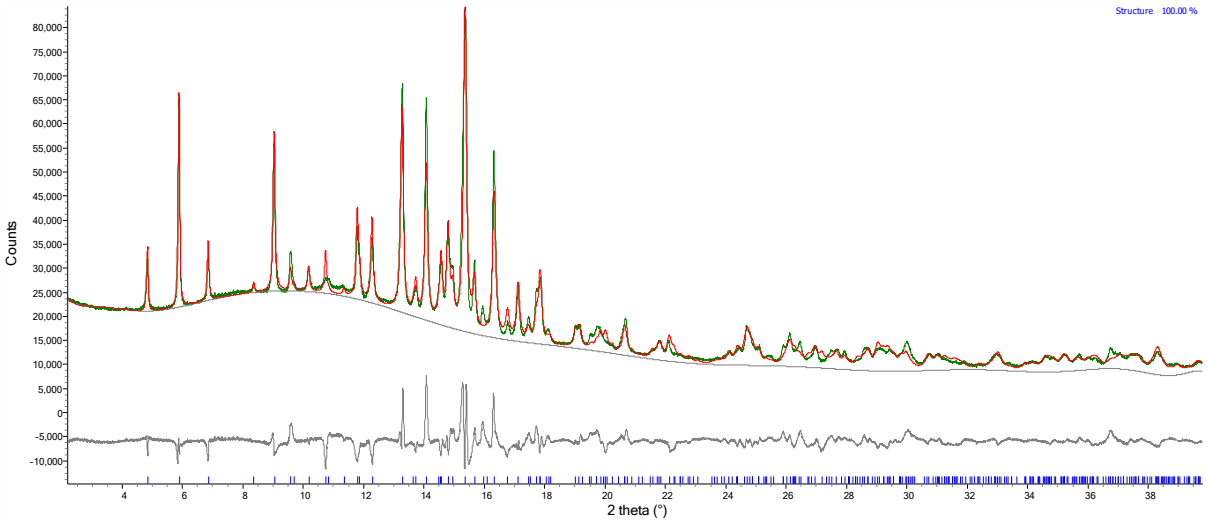

Figure S5.4. Rietveld fit for $Cs_{6.2}$-MER at 40 mbar.

Table S5.3. Refined structure of $Cs_{6.2}$-MER at 40 mbar.

Site	Type	x	y	z	Occ.	Mult.	B_{iso}
Cs1a	Cs	0	0	0	0.47(1)	2	2
Cs2	Cs	0.5	0.695(1)	0	0.29(1)	8	2
Cs3	Cs	0	0.5	0.122(1)	0.59(1)	4	2
O1	O	0.177(1)	0.150(1)	0.190(1)	1	16	1
O2	O	0.130(1)	0.299(1)	0	1	16	1
O3	O	0	0.203(1)	0.174(2)	1	8	1
O5	O	0.712(1)	0.000	0.201(2)	1	8	1
O4	O	0.128(1)	0.321(1)	0.280(1)	1	16	1
Si1	Si	0.108(1)	0.244(1)	0.154(1)	0.81	16	1
Al1	Al	0.108(1)	0.244(1)	0.154(1)	0.19	16	1
Si2	Si	0.715(1)	0.114(1)	0.150(1)	0.81	16	1
Al2	Al	0.715(1)	0.114(1)	0.150(1)	0.19	16	1
C1	C	0.5	0.5	0	0.88(1)	2	4
OC1	O	0.5	0.5	0.117	0.88(1)	4	4

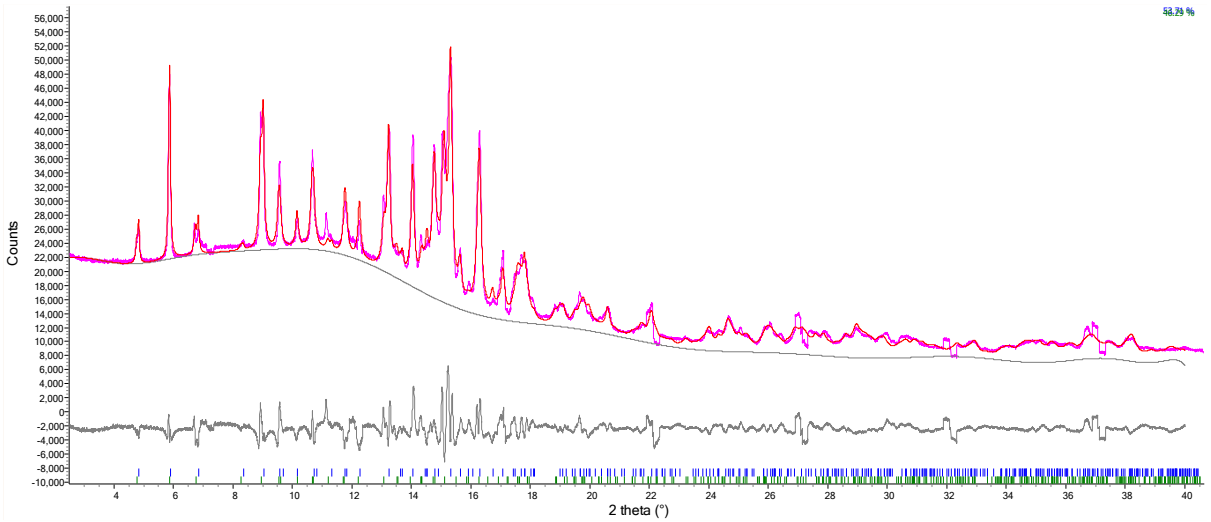

Figure S5.5. Rietveld fit for $Cs_{6.2}$-MER at 100 mbar.

Table S5.4. Refined structure of narrow-pore $Cs_{6.2}$-MER at 100 mbar.

Site	Type	x	y	z	Occ.	Mult.	B_{iso}
Cs1a	Cs	0	0	0	0.47(1)	2	2
Cs2	Cs	0.5	0.698(1)	0	0.28(1)	8	2
Cs3	Cs	0	0.5	0.122(1)	0.59(1)	4	2
O1	O	0.175(2)	0.144(2)	0.177(2)	1	16	1
O2	O	0.130(1)	0.301(2)	0	1	16	1
O3	O	0	0.207(2)	0.168(4)	1	8	1
O5	O	0.696(3)	0	0.197(3)	1	8	1
O4	O	0.132(2)	0.315(2)	0.277(2)	1	16	1
Si1	Si	0.109(1)	0.239(1)	0.149(2)	0.81	16	1
Al1	Al	0.109(1)	0.239(1)	0.149(2)	0.19	16	1
Si2	Si	0.711(1)	0.113(1)	0.151(1)	0.81	16	1
Al2	Al	0.711(1)	0.113(1)	0.151(1)	0.19	16	1
C1	C	0.5	0.5	0	1.00(1)	2	4
OC1	O	0.5	0.5	0.117	1.00(1)	4	4

Table S5.5. Refined structure of wide-pore $Cs_{6.2}$-MER at 100 mbar.

Site	Type	x	y	z	Occ.	Mult.	B_{iso}
Cs1aa	Cs	0	0	0	0.44(1)	4	2
Cs2a	Cs	0.5	0.789(2)	0	0.24(1)	8	2
Cs3a	Cs	0	0.5	0.089(4)	0.27(1)	4	2
O1a	O	0.173(4)	0.173(4)	0.163(4)	1	16	1
O2a	O	0.102(3)	0.303(2)	0	1	16	1
O3a	O	0	0.227(6)	0.206(7)	1	8	1
O5a	O	0.768(7)	0	0.204(7)	1	8	1
O4a	O	0.146(4)	0.348(4)	0.258(6)	1	16	1
Si1a	Si	0.102(3)	0.267(2)	0.160(3)	0.81	16	1
Al1a	Al	0.102(3)	0.267(2)	0.160(3)	0.19	16	1
Si2a	Si	0.733(2)	0.104(3)	0.160(4)	0.81	16	1
Al2a	Al	0.733(2)	0.104(3)	0.160(4)	0.19	16	1
C1a	C	0.5	0.5	0	0.41(6)	2	4
OC1a	O	0.5	0.5	0.117	0.41(6)	4	4
C2a	C	0.172(2)	0	0.5	0.69(2)	8	4
OC2a	O	0.172(2)	-0.082	0.5	0.69(2)	16	4
C3a	C	0	0	0	0.67(4)	2	4
OC3a	O	0	0	0.117	0.67(4)	4	4

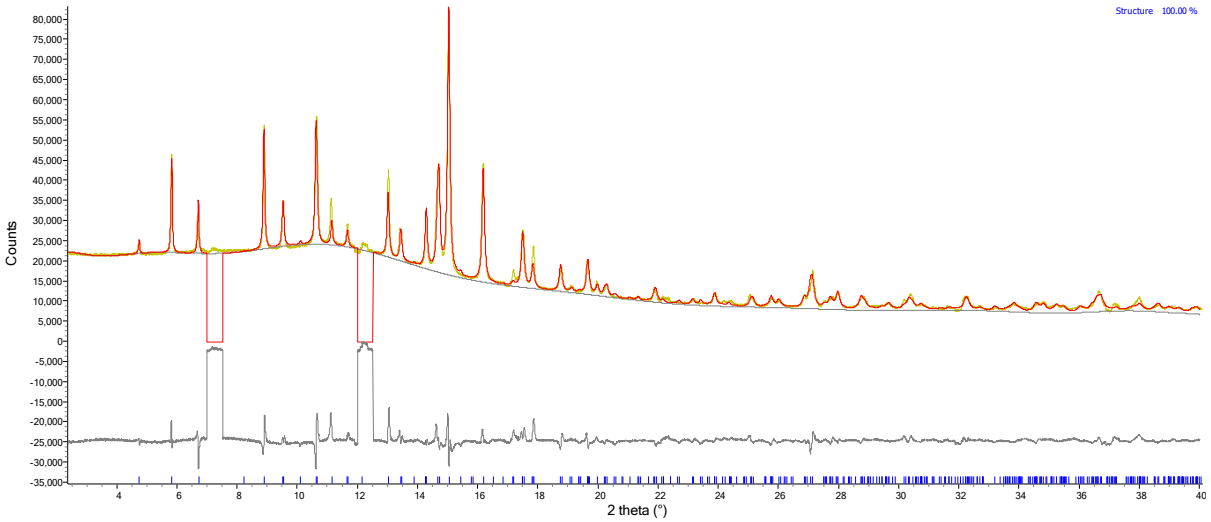

Figure S5.6. Rietveld fit for $Cs_{6.2}$-MER at 230 mbar. Note sections are cut out due to background effects.

NB: sections of pattern are cut out in fit above due to steps present in the background.

Table S5.6. Refined structure of $Cs_{6.2}$-MER at 230 mbar.

Site	Type	x	y	z	Occ.	Mult.	B_{iso}
Cs1	Cs	0	0	-0.264(1)	0.48(1)	4	2
Cs2	Cs	0.5	0.795(1)	0.013(2)	0.21(1)	8	2
Cs3	Cs	0	0.5	0.046(1)	0.31(1)	4	2
O1	O	0.167(2)	0.168(2)	0.175(1)	1	16	1
O2	O	0.114(1)	0.297(1)	0	1	16	1
O3	O	0	0.249(3)	0.200(4)	1	8	1
O5	O	0.753(3)	0	0.198(4)	1	8	1
O4	O	0.155(4)	0.346(4)	0.250(2)	1	16	1
Si1	Si	0.109(1)	0.265(1)	0.157(1)	0.81	16	1
Al1	Al	0.109(1)	0.265(1)	0.157(1)	0.19	16	1
Si2	Si	0.737(1)	0.110(1)	0.156(1)	0.81	16	1
Al2	Al	0.737(1)	0.110(1)	0.156(1)	0.19	16	1
C1	C	0.5	0.5	0	0.33(2)	2	4
OC1	O	0.5	0.5	0.117	0.33(2)	4	4
C2	C	0.167(1)	0	0.5	0.49(1)	8	4
OC2	O	0.167(1)	-0.082	0.5	0.49(1)	16	4
C3	C	0	0	0	0.76(1)	2	4
OC3	O	0	0	0.117	0.76(1)	4	4

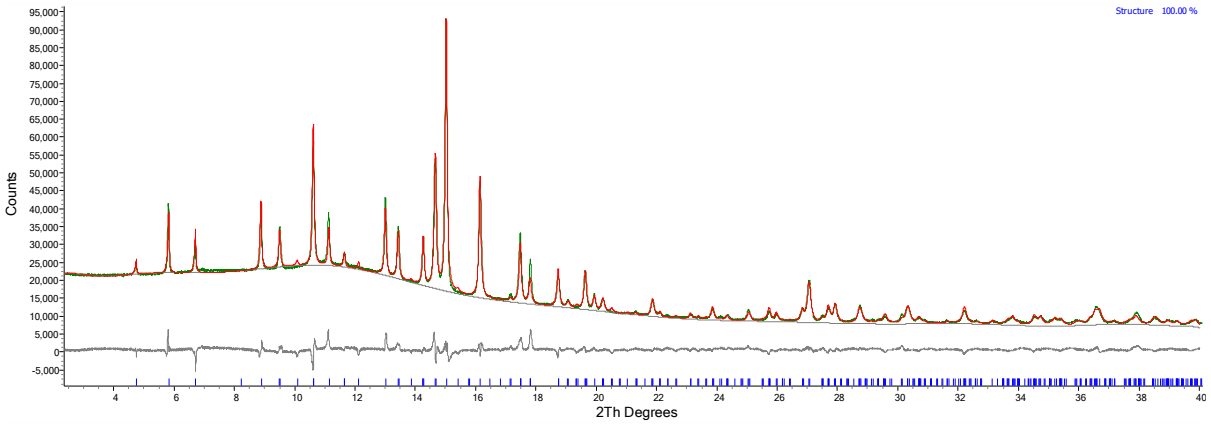

Figure S5.7. Rietveld fit for $Cs_{6.2}$-MER at 880 mbar.

Table S5.7. Refined structure of $Cs_{6.2}$-MER at 880 mbar.

Site	Type	x	y	z	Occ.	Mult.	B_{iso}
Cs1	Cs	0	0	-0.256(1)	0.47(1)	4	2
Cs2	Cs	0.5	0.792(1)	0.002(1)	0.28(2)	8	2
Cs3	Cs	0	0.5	0.055(1)	0.30(1)	4	2
O1	O	0.166(1)	0.166(1)	0.180(1)	1	16	1
O2	O	0.117(1)	0.294(1)	0	1	16	1
O3	O	0	0.249(2)	0.195(3)	1	8	1
O5	O	0.751(2)	0	0.196(3)	1	8	1
O4	O	0.154(16)	0.346(16)	0.250(2)	1	16	1
Si1	Si	0.111(1)	0.263(1)	0.157(1)	0.81	16	1
Al1	Al	0.111(1)	0.263(1)	0.157(1)	0.19	16	1
Si2	Si	0.737(1)	0.111(1)	0.157(1)	0.81	16	1
Al2	Al	0.737(1)	0.111(1)	0.157(1)	0.19	16	1
C1	C	0.5	0.5	0	0.50(1)	2	4
OC1	O	0.5	0.5	0.116	0.50(1)	4	4
C2	C	0.169(1)	0	0.5	0.48(1)	8	4
OC2	O	0.169(1)	-0.082	0.5	0.48(1)	16	4
C3	C	0	0	0	0.81(1)	2	4
OC3	O	0	0	0.116	0.81(1)	4	4

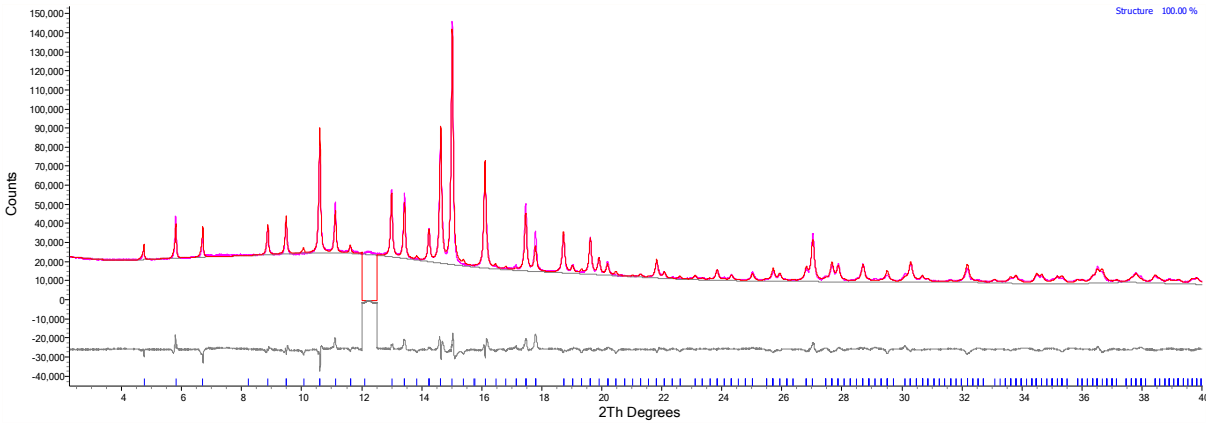

Figure S5.8. Rietveld fit for $Cs_{6.2}$-MER at 2980 mbar. Note sections are cut out due to background effects.

Table S5.8. Refined structure of $Cs_{6.2}$-MER at 2980 mbar.

Site	Type	x	y	z	Occ.	Mult.	B_{iso}
Cs1	Cs	0	0	-0.250(1)	0.46(1)	4	2
Cs2	Cs	0.5	0.790(1)	0.001(1)	0.35(1)	8	2
Cs3	Cs	0	0.5	0.069(1)	0.29(1)	4	2
O1	O	0.163(1)	0.163(1)	0.182(1)	1	16	1
O2	O	0.115(1)	0.295(1)	0	1	16	1
O3	O	0	0.248(2)	0.197(3)	1	8	1
O5	O	0.755(2)	0	0.191(4)	1	8	1
O4	O	0.149(4)	0.3494)	0.254(2)	1	16	1
Si1	Si	0.112(1)	0.263(1)	0.158(1)	0.81	16	1
Al1	Al	0.112(1)	0.263(1)	0.158(1)	0.19	16	1
Si2	Si	0.739(1)	0.112(1)	0.155(1)	0.81	16	1
Al2	Al	0.739(1)	0.112(1)	0.155(1)	0.19	16	1
C1	C	0.5	0.5	0	0.60(1)	2	4
OC1	O	0.5	0.5	0.116	0.60(1)	4	4
C2	C	0.177(1)	0	0.5	0.52(1)	8	4
OC2	O	0.177(1)	-0.082	0.5	0.52(1)	16	4
C3	C	0	0	0	0.86(1)	2	4
OC3	O	0	0	0.116	0.86(1)	4	4

S5.2. $K_{6.2}$-MER

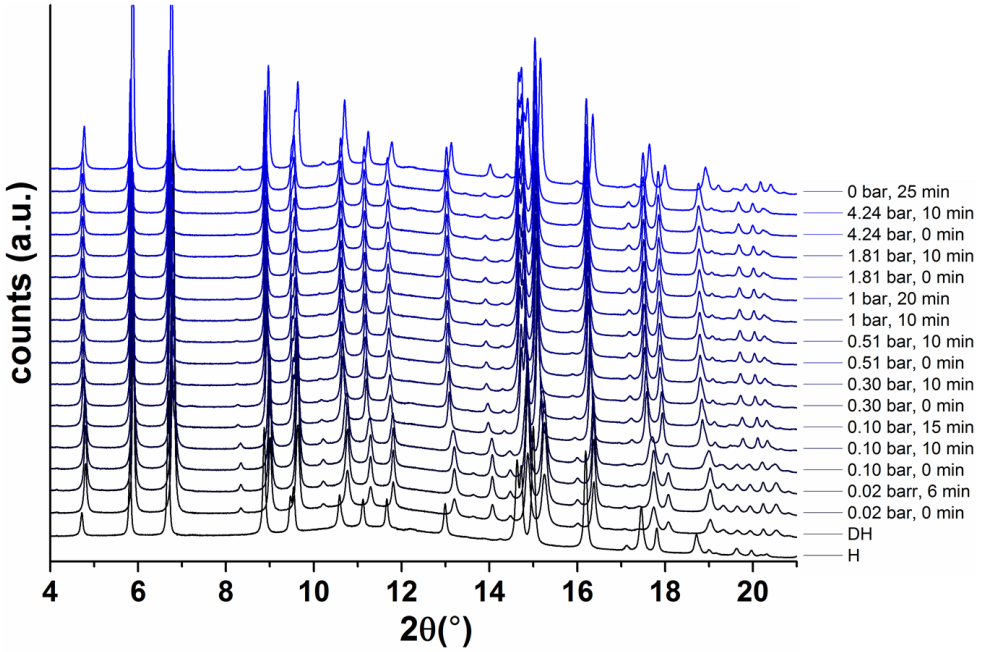

Figure S5.9. Synchrotron in situ VPXRD data for $K_{6.2}$-MER.

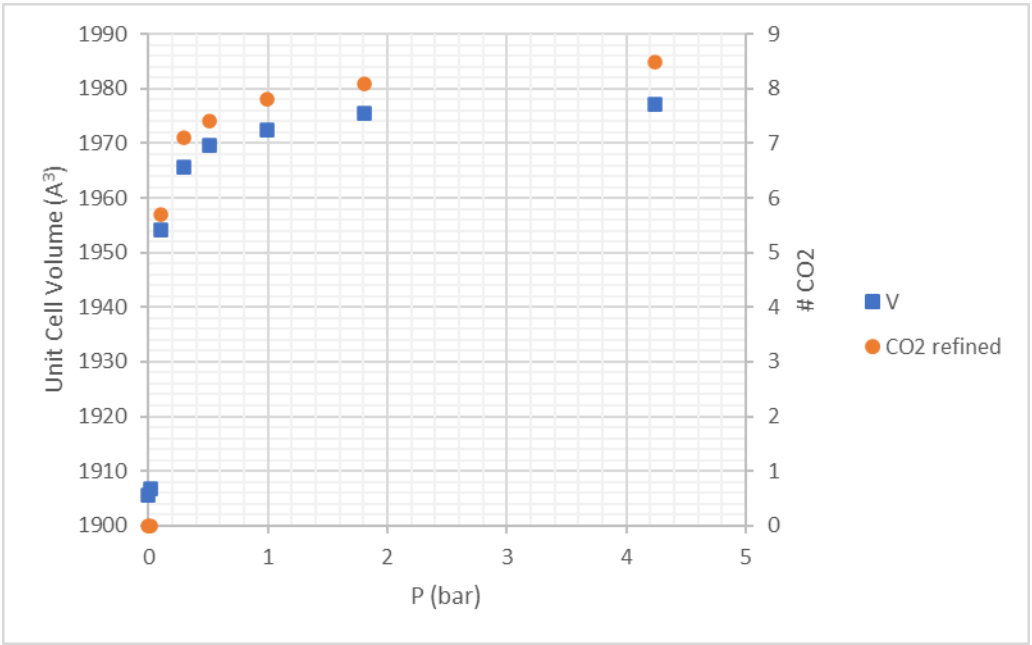

Figure S5.10. Unit cell volume and CO_2 content (molecules uc^{-1}) data from $K_{6.2}$-MER refinements with pressure.

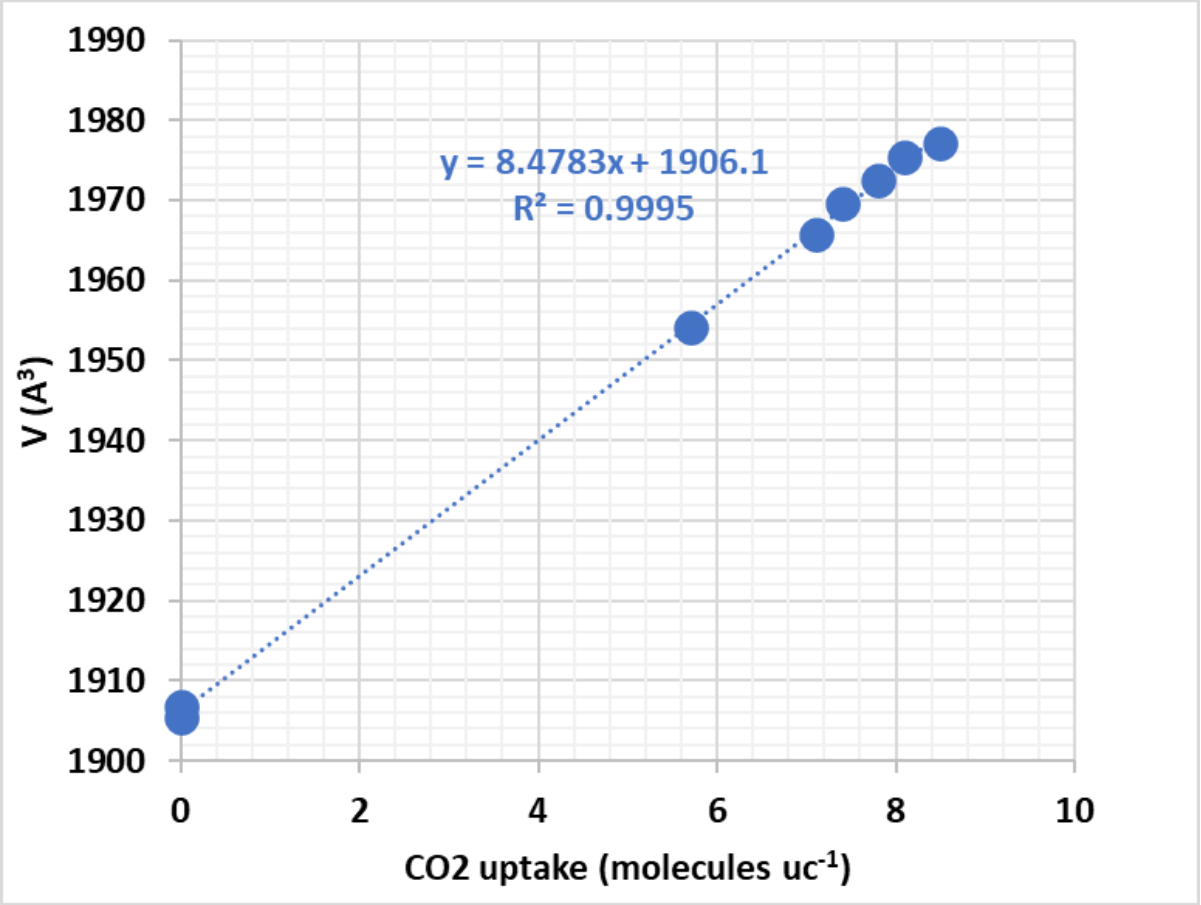

Figure S5.11. Volume dependency on CO_2 uptake.

Table S5.9. Crystallography of $K_{6.2}$-MER under CO_2 exposure.

Sample	**$K_{6.2}$-MER**	**$K_{6.2}$-MER (20 mbar)**	**$K_{6.2}$-MER (100 mbar)**
Unit Cell	$K_{6.1}[Si_{25.8}Al_{6.2}O_{64}]$	$K_{6.4}[Si_{25.8}Al_{6.2}O_{64}]$	$K_{6.2}[Si_{25.8}Al_{6.2}O_{64}]$ $.(CO_2)_{5.7}$
T (K)	298	298	298
Space Group	*Pmmn*	*Pmmn*	*P*4_2/*nmc*
X-ray Source	I11	I11	I11
λ (Å)	0.826398	0.826398	0.826398
***a* (Å)**	13.950(1)	13.948(1)	14.069(1)
***b* (Å)**	13.894(1)	13.901(1)	
***c* (Å)**	9.831(1)	9.834(1)	9.873(1)
***V* (Å^3)**	1905(1)	1907(1)	1954(1)
R_{wp}	2.4	2.8	2.8
R_p	1.9	2.1	2.1
χ^2	24	34	33
Sample	**$K_{6.2}$-MER (300 mbar)**	**$K_{6.2}$-MER (510 mbar)**	**$K_{6.2}$-MER (990 mbar)**
Unit Cell	$K_{6.3}[Si_{25.8}Al_{6.2}O_{64}]$ $.(CO_2)_{7.1}$	$K_{6.4}[Si_{25.8}Al_{6.2}O_{64}]$ $.(CO_2)_{7.4}$	$K_{6.3}[Si_{25.8}Al_{6.2}O_{64}]$ $.(CO_2)_{7.8}$
T (K)	298	298	298
Space Group	*P*4_2/*nmc*	*P*4_2/*nmc*	*P*4_2/*nmc*
X-ray Source	I11	I11	I11
λ (Å)	0.826398	0.826398	0.826398
***a* (Å)**	14.094(1)	14.102(1)	14.107(1)
***c* (Å)**	9.896(1)	9.904(1)	9.912(1)
***V* (Å^3)**	1966(1)	1970(1)	1973(1)
R_{wp}	2.9	2.9	2.9
R_p	2.2	2.2	2.2
χ^2	35	37	36
Sample	**$K_{6.2}$-MER (1810 mbar)**	**$K_{6.2}$-MER (4240 mbar)**	
Unit Cell	$K_{6.3}[Si_{25.8}Al_{6.2}O_{64}]$ $.(CO_2)_{8.1}$	$K_{6.3}[Si_{25.8}Al_{6.2}O_{64}]$ $.(CO_2)_{8.5}$	
T (K)	298	298	
Space Group	*P*4_2/*nmc*	*P*4_2/*nmc*	
X-ray Source	I11	I11	
λ (Å)	0.826398	0.826398	
***a* (Å)**	14.113(1)	14.112(1)	
***c* (Å)**	9.918(1)	9.928(1)	
***V* (Å^3)**	1975(1)	1977(1)	
R_{wp}	3.0	2.9	
R_p	2.2	2.1	
χ^2	38	36	

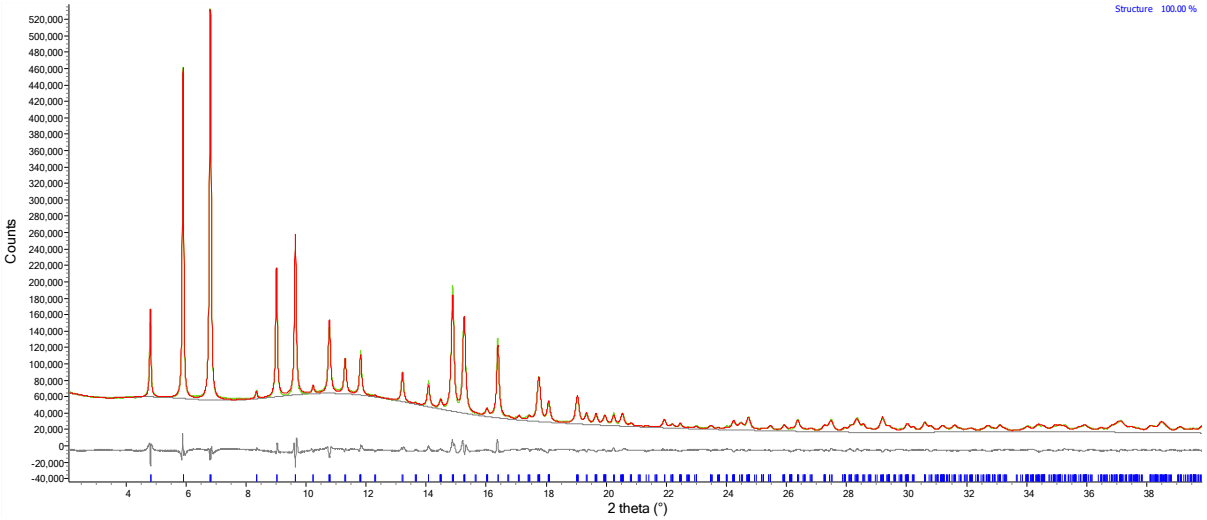

Figure S5.12. Rietveld fit for $K_{6.2}$-MER at 20 mbar.

Table S5.10. Refined structure of $K_{6.2}$-MER at 20 mbar.

Site	Type	x	y	z	Occ.	Mult.	B_{iso}
K1	K	0	0	0.531(3)	0.24(1)	2	2
K11	K	0	0	0.082(2)	0.46(1)	2	2
K2a	K	0.5	-0.212(1)	0.260(1)	0.59(1)	4	2
K2b	K	0.657(1)	0	0.789(1)	1	4	2
O1	O	-0.177(1)	0.156(1)	0.067(2)	1	8	1
O2	O	0.157(1)	0.183(1)	0.435(2)	1	8	1
O3	O	-0.119(1)	-0.300(1)	0.231(2)	1	8	1
O4	O	0	-0.211(1)	0.060(2)	1	4	1
O5	O	0	-0.287(1)	0.441(2)	1	4	1
O6	O	0.139(1)	-0.329(1)	-0.032(2)	1	8	1
O7	O	-0.330(1)	0.132(1)	0.529(2)	1	8	1
O8	O	0.296(1)	-0.118(1)	0.272(2)	1	8	1
O9	O	-0.204(1)	0	0.441(1)	1	4	1
O10	O	-0.282(1)	0	0.061(1)	1	4	1
Si1	Si	-0.110(1)	0.291(1)	0.395(1)	0.81	8	1
Al1	Al	-0.110(1)	0.291(1)	0.395(1)	0.19	8	1
Si2	Si	-0.107(1)	-0.247(1)	0.084(1)	0.81	8	1
Al2	Al	-0.107(1)	-0.247(1)	0.084(1)	0.19	8	1
Si3	Si	-0.228(1)	0.385(1)	-0.112(1)	0.81	8	1
Al3	Al	-0.228(1)	0.385(1)	-0.112(1)	0.19	8	1
Si4	Si	0.252(1)	0.393(1)	0.578(1)	0.81	8	1
Al4	Al	0.252(1)	0.393(1)	0.578(1)	0.19	8	1

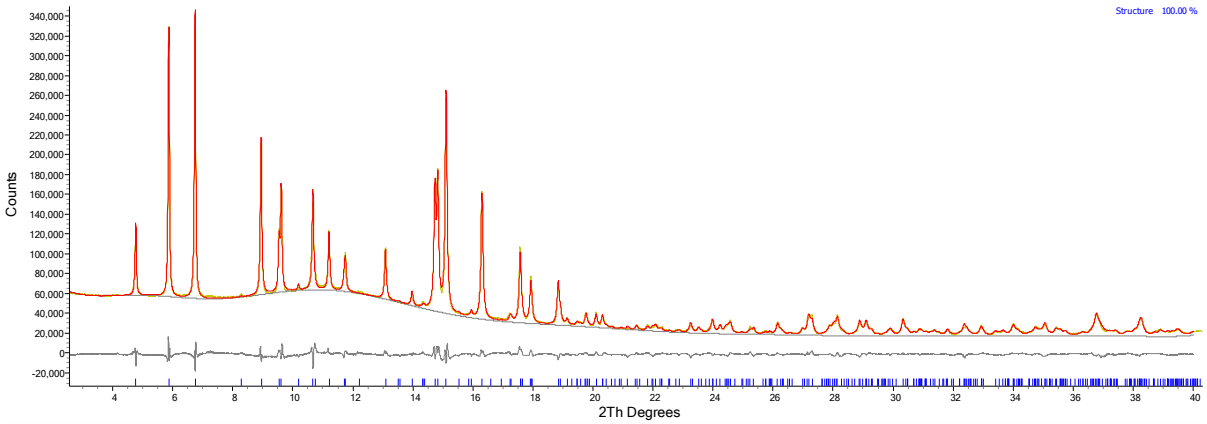

Figure S5.13. Rietveld fit for $K_{6.2}$-MER at 100 mbar.

Table S5.11. Refined structure of $K_{6.2}$-MER at 100 mbar.

Site	Type	x	y	z	Occ.	Mult.	B_{iso}
K1	K	0	0	0.752(1)	0.30(1)	4	2
K2	K	0.5	0.824(1)	0.021(1)	0.63(1)	8	2
O1	O	0.160(1)	0.175(1)	0.185(1)	1	16	1
O2	O	0.124(1)	0.298(1)	0	1	16	1
O3	O	0	0.266(1)	0.201(1)	1	8	1
O5	O	0.780(1)	0	0.194(1)	1	8	1
O4	O	0.162(1)	0.366(1)	0.235(1)	1	16	1
Si1	Si	0.112(2)	0.277(2)	0.153(1)	1	16	1
Al1	Al	0.112(2)	0.277(2)	0.153(1)	1	16	1
Si2	Si	0.745(1)	0.109(1)	0.164(1)	1	16	1
Al2	Al	0.745(1)	0.109(1)	0.164(1)	1	16	1
C1	C	0.5	0.5	0	0.37(1)	2	4
OC1	O	0.5	0.5	0.117	0.37(1)	4	4
C2	C	0.148(1)	0	0.5	0.22(2)	8	4
OC2	O	0.148(1)	-0.082	0.5	0.22(2)	16	4
C3	C	0	0.5	0.208(2)	0.47(1)	4	4
OC3	O	0	0.5	0.325(2)	0.47(1)	4	4
OC3a	O	0	0.5	0.090(2)	0.47(1)	4	4
C4	C	0	0	0	0.66(1)	2	4
OC4	O	0	0	0.117	0.66(1)	4	4

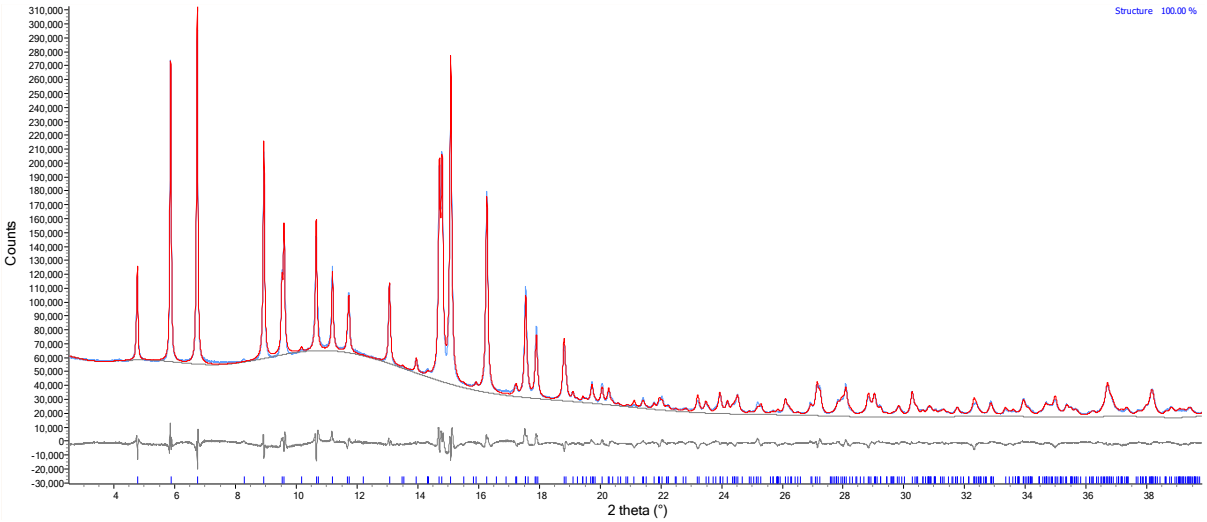

Figure S5.14. Rietveld fit for $K_{6.2}$-MER at 300 mbar.

Table S5.12. Refined structure of $K_{6.2}$-MER at 300 mbar.

Site	Type	x	y	z	Occ.	Mult.	B_{iso}
K1	K	0	0	0.744(1)	0.27(1)	4	2
K2	K	0.5	0.826(1)	0.020(1)	0.65(1)	8	2
O1	O	0.160(1)	0.177(1)	0.185(1)	1	16	1
O2	O	0.1252)	0.298(1)	0	1	16	1
O3	O	0	0.260(1)	0.202(1)	1	8	1
O5	O	0.780(1)	0	0.195(1)	1	8	1
O4	O	0.159(1)	0.366(1)	0.237(1)	1	16	1
Si1	Si	0.111(1)	0.276(1)	0.154(1)	1	16	1
Al1	Al	0.111(1)	0.276(1)	0.154(1)	1	16	1
Si2	Si	0.744(1)	0.109(1)	0.163(1)	1	16	1
Al2	Al	0.744(1)	0.109(1)	0.163(1)	1	16	1
C1	C	0.5	0.5	0	0.41(1)	2	4
OC1	O	0.5	0.5	0.117	0.41(1)	4	4
C2	C	0.152(1)	0	0.5	0.33(1)	8	4
OC2	O	0.152(1)	-0.082	0.5	0.33(1)	16	4
C3	C	0	0.5	0.213(2)	0.54(1)	4	4
OC3	O	0	0.5	0.330(2)	0.54(1)	4	4
OC3a	O	0	0.5	0.096(2)	0.54(1)	4	4
C4	C	0	0	0	0.76(1)	2	4
OC4	O	0	0	0.117	0.76(1)	4	4

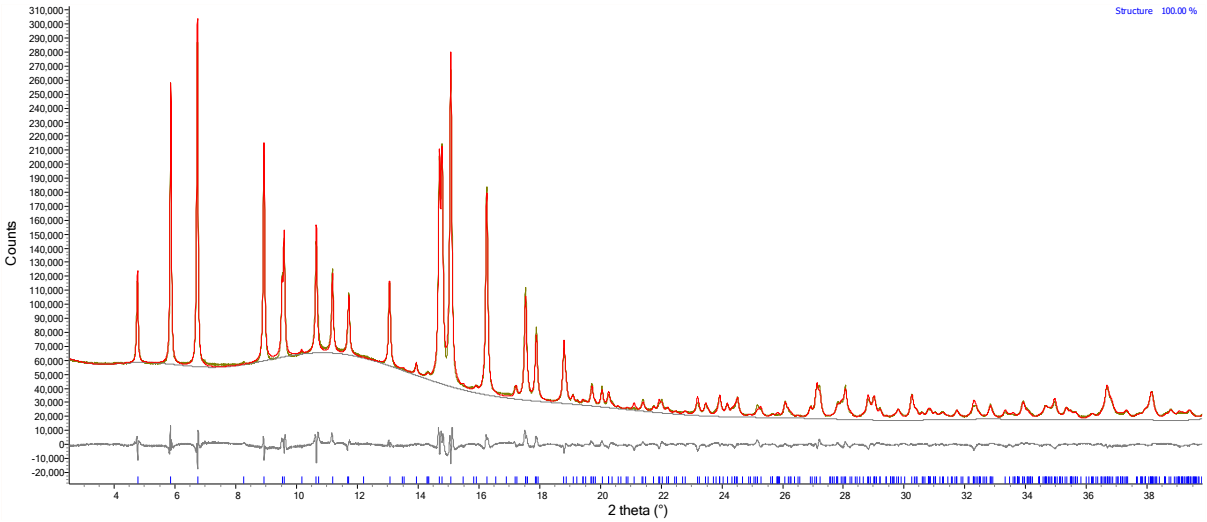

Figure S5.15. Rietveld fit for $K_{6.2}$-MER at 510 mbar.

Table S5.13. Refined structure of $K_{6.2}$-MER at 510 mbar.

Site	Type	x	y	z	Occ.	Mult.	B_{iso}
K1	K	0	0	0.742(1)	0.27(1)	4	2
K2	K	0.5	0.827(1)	0.019(1)	0.66(1)	8	2
O1	O	0.159(1)	0.177(1)	0.185(1)	1	16	1
O2	O	0.126(1)	0.298(1)	0	1	16	1
O3	O	0	0.258(1)	0.203(1)	1	8	1
O5	O	0.778(1)	0	0.195(1)	1	8	1
O4	O	0.158(1)	0.365(1)	0.239(1)	1	16	1
Si1	Si	0.111(1)	0.275(1)	0.155(1)	1	16	1
Al1	Al	0.111(1)	0.275(1)	0.155(1)	1	16	1
Si2	Si	0.743(1)	0.109(1)	0.162(1)	1	16	1
Al2	Al	0.743(1)	0.109(1)	0.162(1)	1	16	1
C1	C	0.5	0.5	0	0.42(1)	2	4
OC1	O	0.5	0.5	0.117	0.42(1)	4	4
C2	C	0.151(1)	0	0.5	0.35(1)	8	4
OC2	O	0.151(1)	-0.082	0.5	0.35(1)	16	4
C3	C	0	0.5	0.208(2)	0.56(1)	4	4
OC3	O	0	0.5	0.325(2)	0.56(1)	4	4
OC3a	O	0	0.5	0.091(2)	0.56(1)	4	4
C4	C	0	0	0	0.78(1)	2	4
OC4	O	0	0	0.117	0.78(1)	4	4

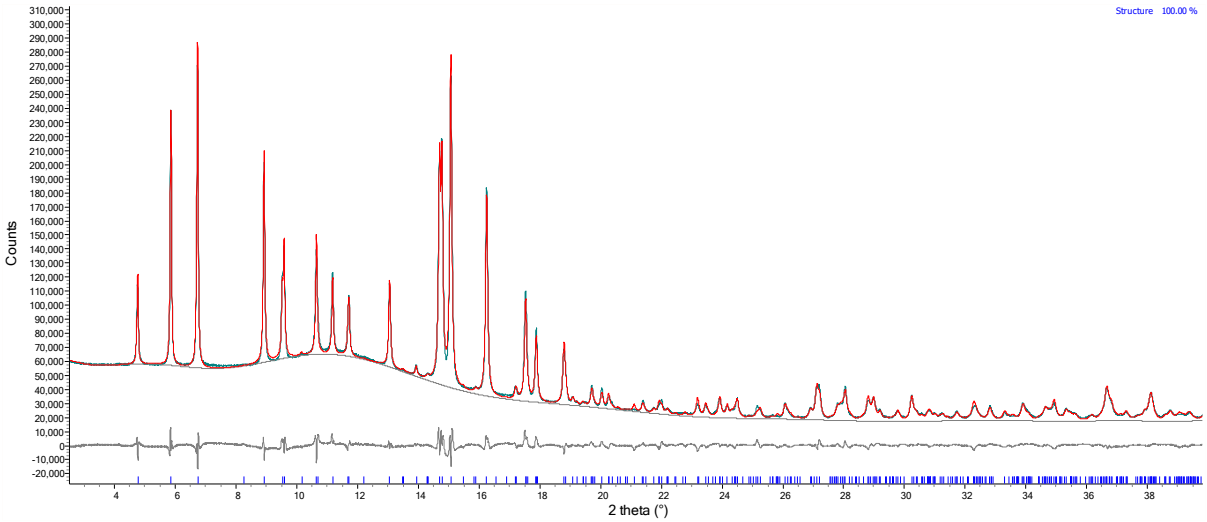

Figure S5.16. Rietveld fit for $K_{6.2}$-MER at 990 mbar.

Table S5.14. Refined structure of $K_{6.2}$-MER at 990 mbar.

Site	Type	x	y	z	Occ.	Mult.	B_{iso}
K1	K	0	0	0.740(1)	0.26(1)	4	2
K2	K	0.5	0.827(1)	0.019(1)	0.66(1)	8	2
O1	O	0.159(1)	0.176(1)	0.185(1)	1	16	1
O2	O	0.126(1)	0.298(1)	0	1	16	1
O3	O	0	0.257(1)	0.203(1)	1	8	1
O5	O	0.777(1)	0	0.195(1)	1	8	1
O4	O	0.157(1)	0.365(1)	0.241(1)	1	16	1
Si1	Si	0.111(1)	0.275(1)	0.155(1)	1	16	1
Al1	Al	0.111(1)	0.275(1)	0.155(1)	1	16	1
Si2	Si	0.743(1)	0.109(1)	0.162(1)	1	16	1
Al2	Al	0.743(1)	0.109(1)	0.162(1)	1	16	1
C1	C	0.5	0.5	0	0.42(1)	2	4
OC1	O	0.5	0.5	0.117	0.42(1)	4	4
C2	C	0.152(1)	0	0.5	0.38(1)	8	4
OC2	O	0.152(1)	-0.082	0.5	0.38(1)	16	4
C3	C	0	0.5	0.207(2)	0.58(1)	4	4
OC3	O	0	0.5	0.324(2)	0.58(1)	4	4
OC3a	O	0	0.5	0.089(2)	0.58(1)	4	4
C4	C	0	0	0	0.80(1)	2	4
OC4	O	0	0	0.117	0.80(1)	4	4

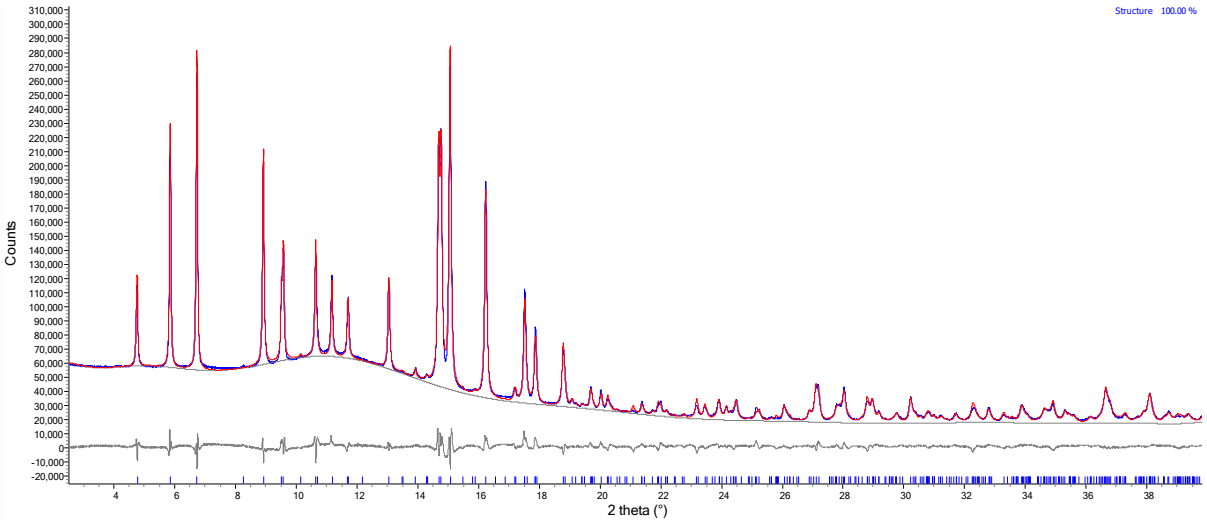

Figure S5.17. Rietveld fit for $K_{6.2}$-MER at 1810 mbar.

Table S5.15. Refined structure of $K_{6.2}$-MER at 1810 mbar.

Site	Type	x	y	z	Occ.	Mult.	B_{iso}
K1	K	0	0	0.739(1)	0.26(1)	4	2
K2	K	0.5	0.827(1)	0.018(1)	0.66(1)	8	2
O1	O	0.159(1)	0.177(1)	0.185(1)	1	16	1
O2	O	0.126(1)	0.298(1)	0	1	16	1
O3	O	0	0.256(1)	0.203(1)	1	8	1
O5	O	0.776(1)	0	0.195(1)	1	8	1
O4	O	0.156(1)	0.364(1)	0.242(1)	1	16	1
Si1	Si	0.111(1)	0.275(1)	0.155(1)	1	16	1
Al1	Al	0.111(1)	0.275(1)	0.155(1)	1	16	1
Si2	Si	0.743(1)	0.109(1)	0.162(1)	1	16	1
Al2	Al	0.743(1)	0.109(1)	0.162(1)	1	16	1
C1	C	0.5	0.5	0	0.42(1)	2	4
OC1	O	0.5	0.5	0.117	0.42(1)	4	4
C2	C	0.152(1)	0	0.5	0.41(1)	8	4
OC2	O	0.152(1)	-0.082	0.5	0.41(1)	16	4
C3	C	0	0.5	0.207(2)	0.61(1)	4	4
OC3	O	0	0.5	0.324(2)	0.61(1)	4	4
OC3a	O	0	0.5	0.090(2)	0.61(1)	4	4
C4	C	0	0	0	0.81(1)	2	4
OC4	O	0	0	0.117	0.81(1)	4	4

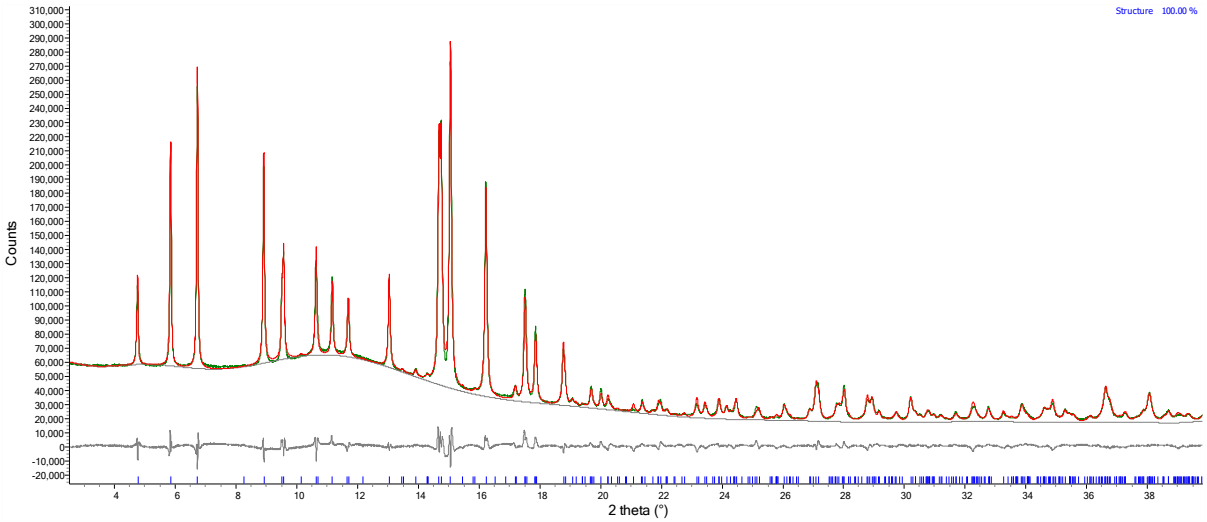

Figure S5.18. Rietveld fit for $K_{6.2}$-MER at 4240 mbar.

Table S5.16. Refined structure of $K_{6.2}$-MER at 4240 mbar.

Site	Type	x	y	z	Occ.	Mult.	B_{iso}
K1	K	0	0	0.738(1)	0.26(1)	4	2
K2	K	0.5	0.827(1)	0.017(1)	0.66(1)	8	2
O1	O	0.159(1)	0.177(1)	0.185(1)	1	16	1
O2	O	0.127(1)	0.298(1)	0	1	16	1
O3	O	0	0.254(1)	0.203(1)	1	8	1
O5	O	0.775(1)	0	0.195(1)	1	8	1
O4	O	0.155(1)	0.363(1)	0.244(1)	1	16	1
Si1	Si	0.111(1)	0.274(1)	0.155(1)	1	16	1
Al1	Al	0.111(1)	0.274(1)	0.155(1)	1	16	1
Si2	Si	0.742(1)	0.109(1)	0.161(1)	1	16	1
Al2	Al	0.742(1)	0.109(1)	0.161(1)	1	16	1
C1	C	0.5	0.5	0	0.43(1)	2	4
OC1	O	0.5	0.5	0.117	0.43(1)	4	4
C2	C	0.153(1)	0	0.5	0.43(1)	8	4
OC2	O	0.153(1)	-0.082	0.5	0.43(1)	16	4
C3	C	0	0.5	0.209(2)	0.65(1)	4	4
OC3	O	0	0.5	0.326(2)	0.65(1)	4	4
OC3a	O	0	0.5	0.092(2)	0.65(1)	4	4
C4	C	0	0	0	0.82(1)	2	4
OC4	O	0	0	0.117	0.82(1)	4	4

S6. $Na_{4.0}K_{2.2}$-MER VPXRD data

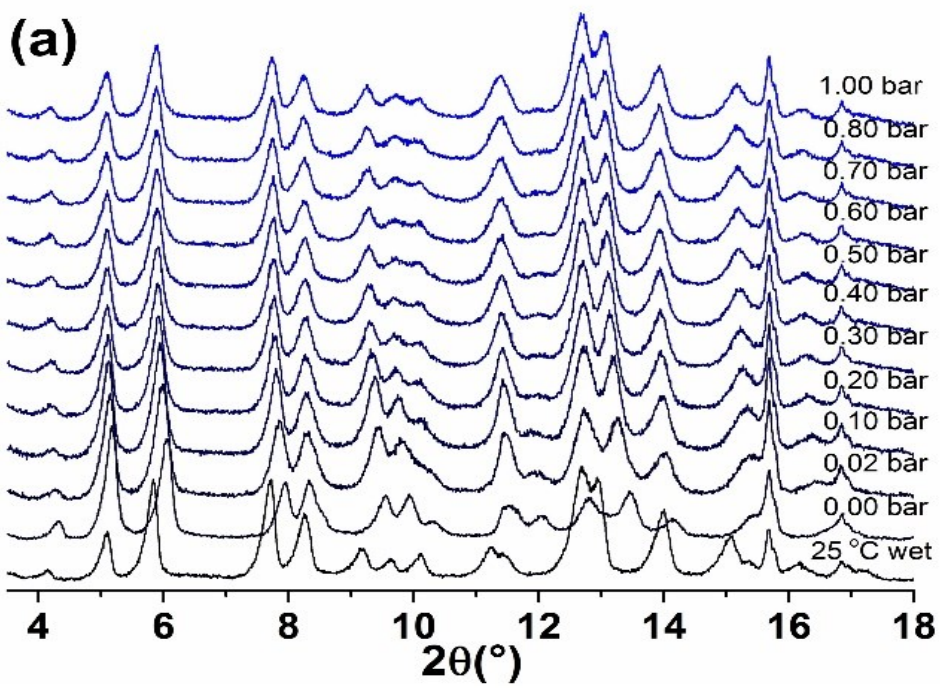

Figure S 6.1. Lab-based in situ VPXRD data for $Na_{4.0}K_{2.2}$-MER: patterns obtained at 298 K, at given p_{CO2} values.

S7 Kinetic Measurements using the Zero Length Column technique

ZLC analysis was carried out as described in the experimental section and analysis was carried out much as was described in Georgieva *et al,*[1] and a more detailed description of the method is provided by Ruthven, Eic and Brandani.[2,3]

S 7.1 Powder samples of pure cation MER

Figure S7.1 shows the normalised desorption data for $Na_{6.2}$-MER in 10% CO_2 in helium at ambient pressure (i.e. pCO_2 = 0.1 bar) and at T = 298 K versus time. Associated q_0 values are *ca.*1.9 mol/kg, slightly lower than expected from CO_2 adsorption isotherms, likely due to lower activation temperature of 523 K used prior to ZLC measurement.

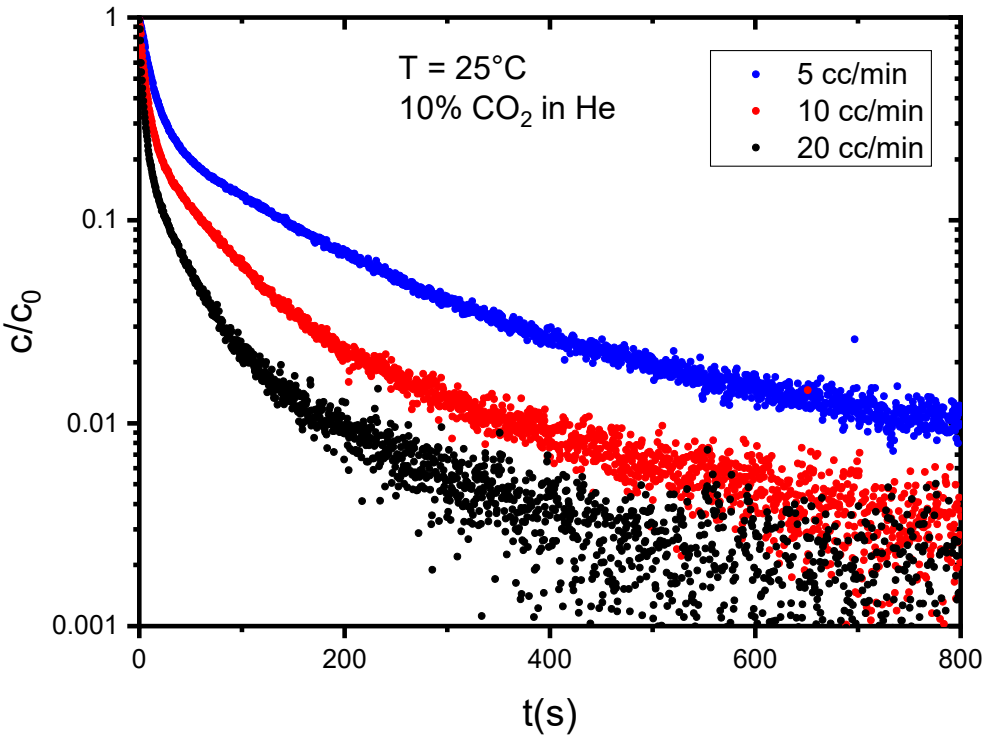

Figure S7.1. Normalised concentration c/c_0 vs. time for $Na_{6.2}$-MER.

Kinetic control is more evident after carrying out deconvolution to show the lack of overlap for different flow rates in desorption behaviour at low concentrations more clearly, as seen in Figure S. Long-time analysis suggests D/R^2 = 8.6 × 10–4 s^{-1} at 25°C. Carrying out ZLC experiments at multiple temperatures and determining the diffusivity values, listed in Table S,allows the activation energy, E_{act}, to be found as shown in Figure . For $Na_{6.2}$-MER, E_{act} was found to be 27 kJ/mol.

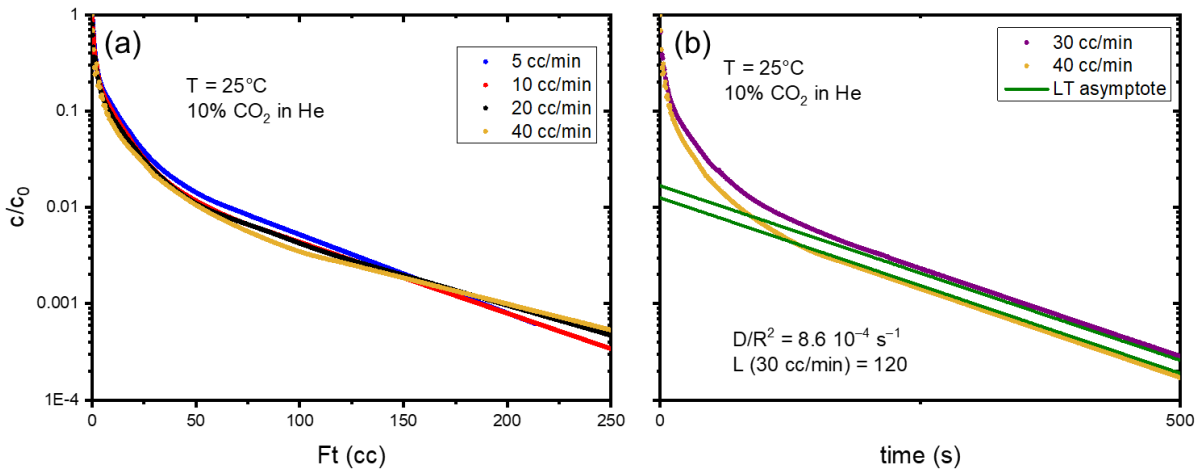

Figure S7.2. Deconvoluted, normalised concentration c/c_0 vs. (a) eluted volume and (b) time for $Na_{6.2}$-MER. A range of flow rates is shown in (a) whilst long time analysis for higher flow rates is shown in (b), including fits to the long-time behaviour via an analytic model.

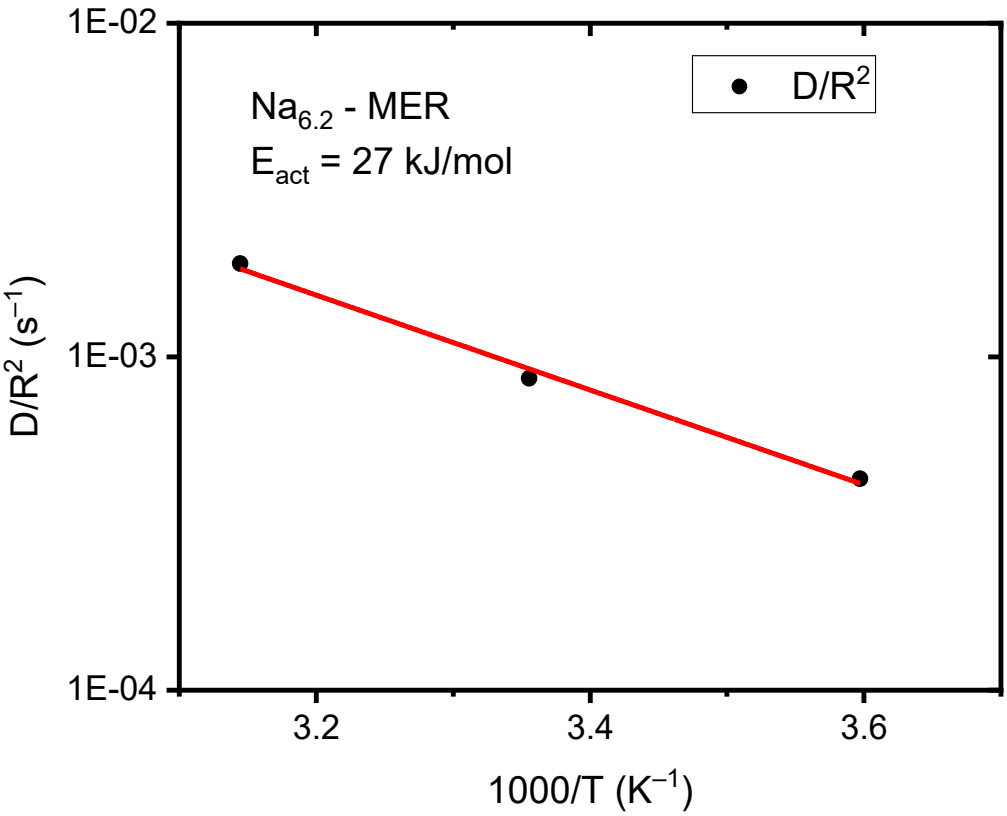

Figure S7.3 Diffusivity values for $Na_{6.2}$-MER at different temperatures allows for an estimation of its activation energy.

Table S7.1. Diffusivity values for $Na_{6.2}$-MER at varying temperatures.

Temperature (K)	278	298	318
D/R^2 (s^{-1})	4.3×10^{-4}	8.6×10^{-4}	1.9×10^{-3}

The normalised desorption behaviour of $K_{6.2}$-MER in 10% CO_2 in He at 308 K is shown in Figure S7.4. Values of q_0 are *ca*. 2.0 mol/kg.

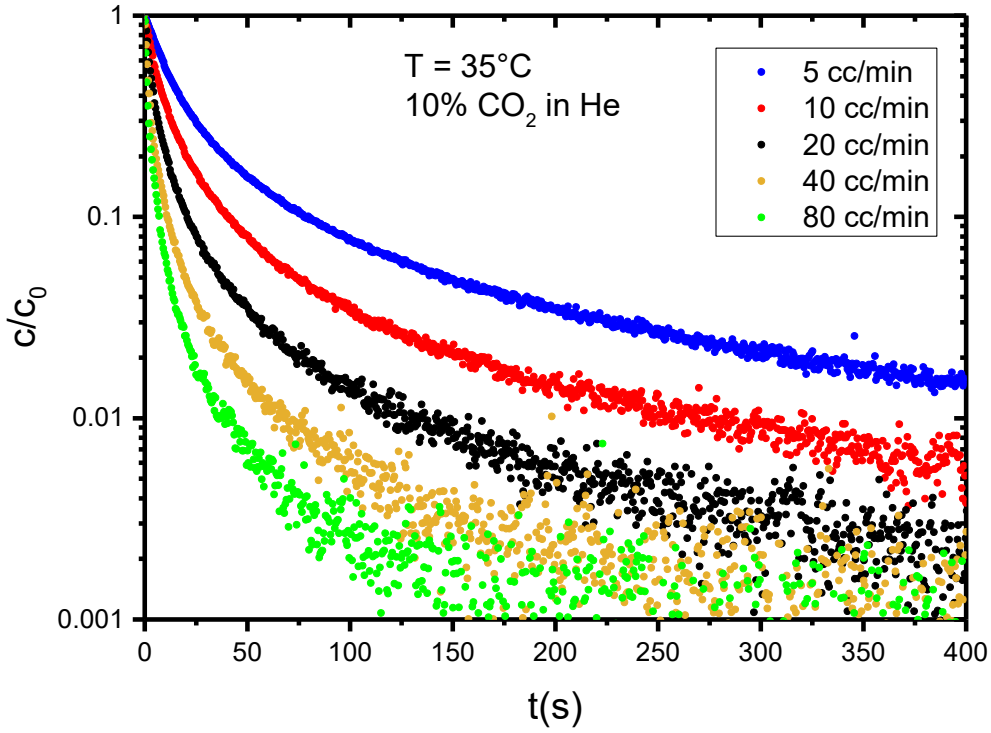

Figure S7.4. Normalised concentration c/c_0 vs. time for $K_{6.2}$-MER.

By plotting against the eluted volume, as shown in Figure S7.5, it can be seen that the different flow rates overlap and so the sample is under equilibrium control for the range of temperatures investigated here (288 – 328 K). The kinetic behaviour of this sample is therefore too rapid for measurement using our setup.

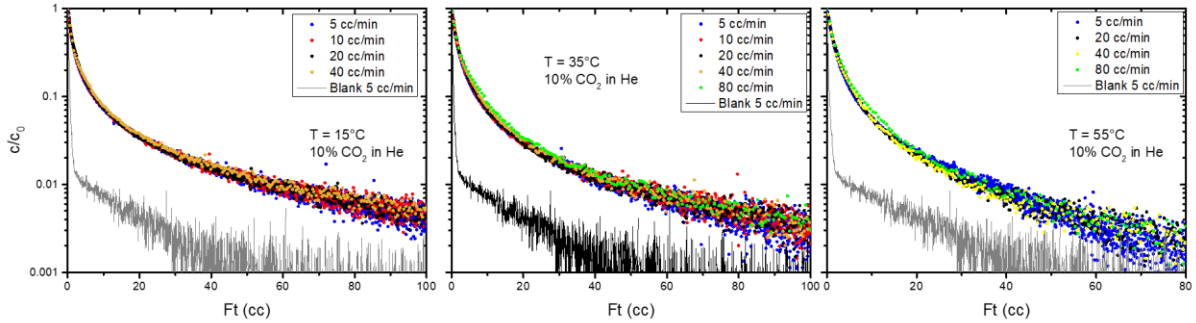

Figure S7.5. Normalised concentration c/c_0 vs. eluted volume for $K_{6.2}$-MER at 288 (left), 308 (middle) and 328 K (right). Overlap of different flow rate experiments shows equilibrium control for all runs.

The c/c_0 for $Cs_{6.2}$-MER in 10% CO_2 in helium at ambient pressure (i.e. pCO_2 = 0.1 bar) and at T = 308 K versus time is shown in Figure S. Associated q_0 values are *ca*. 1.2 mol/kg.

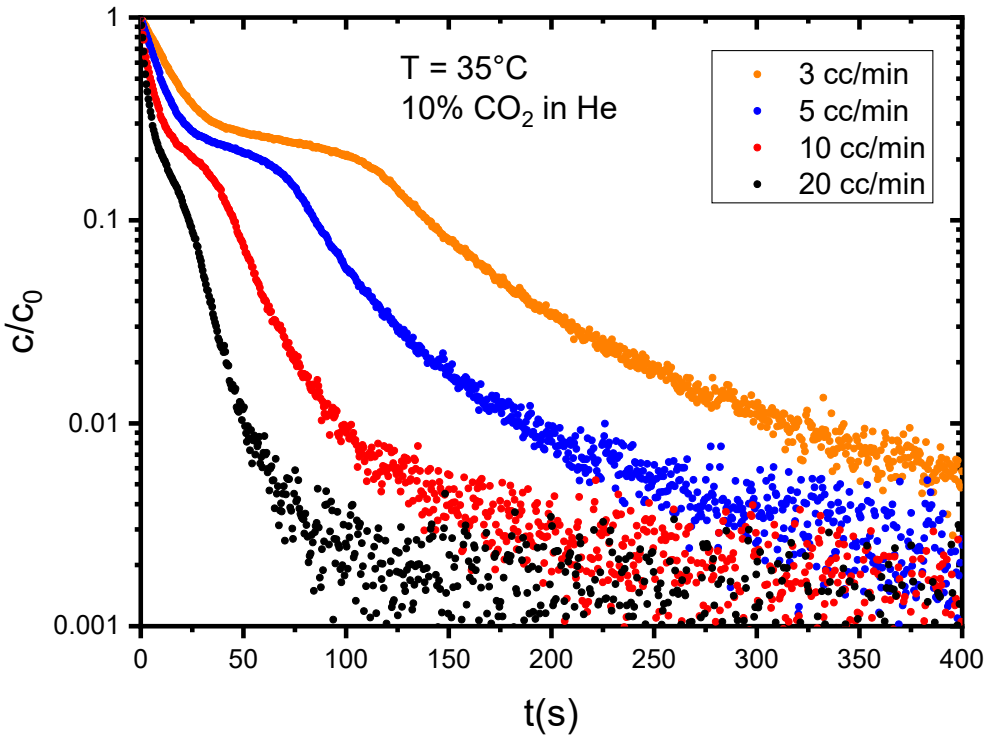

Figure S 7.6 Normalised concentration c/c_0 vs. time for $Cs_{6.2}$-MER.

Plotting against eluted volume, as shown in Figure, consists of an initial overlapping region, indicating equilibrium control and rapid kinetics, before a divergent region indicative of kinetic control on a longer timescale, after an inflection point at c/c_0 *ca*. 0.3.

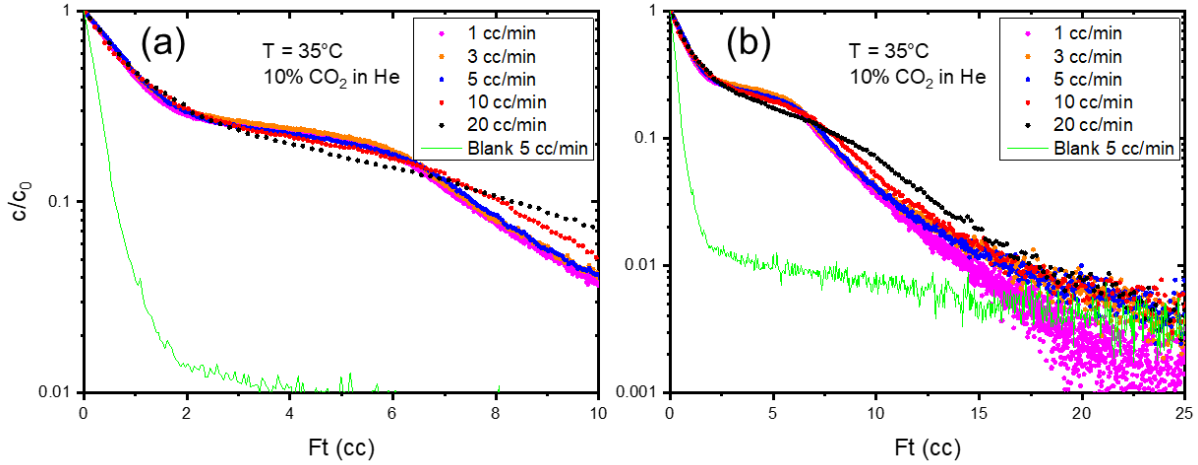

Figure S7.7. Normalised concentration c/c_0 vs. eluted volume for $Cs_{6.2}$-MER at 308 K: (a) short time expansion of the (b) longer time run, showing different regimes. Desorption appears to become kinetically limited at the inflection point, c/c_0 ~ 0.3.

Carrying out deconvolution and fitting the data, shown in Figure, as before for $Na_{6.2}$-MER, at varying temperatures allows us to extract kinetic parameters, listed in Table S, and subsequently determine E_{act}, as seen in Figure. For the lower temperature of 268 K, a lower pCO_2 of 0.01 bar in helium was required. E_{act} was found to be 51 kJ/mol, which seems high and may be due to the structural change.

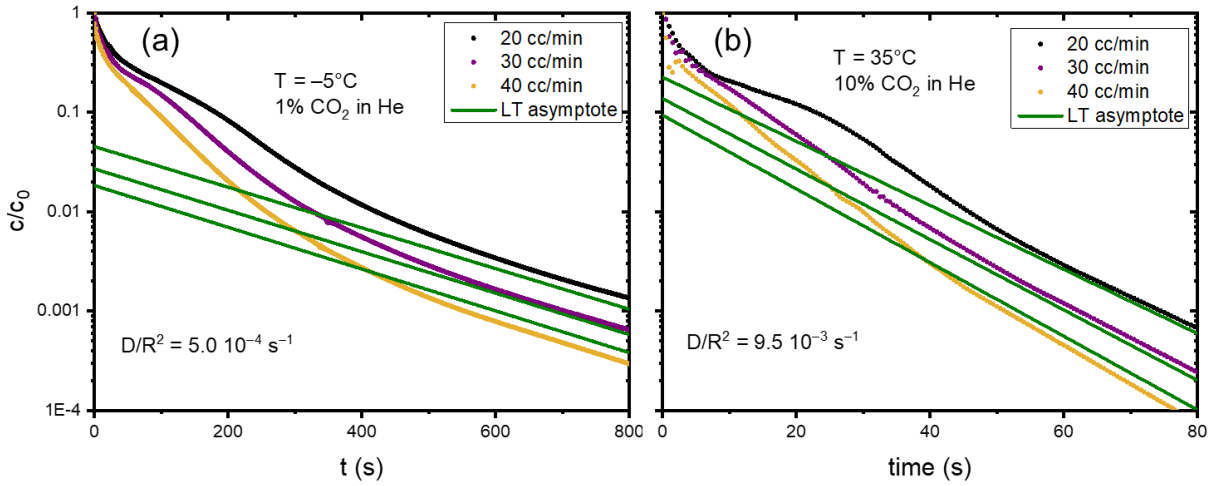

Figure 7.8. Deconvoluted, normalised concentration c/c_0 vs. time for $Cs_{6.2}$-MER. A range of flow rates is shown including fits to the long-time behaviour via an analytic model.

Table S7.2. Diffusivity values for $Cs_{6.2}$-MER at varying temperatures.

Temperature (K)	268	288	308
D/R^2 (s^{-1})	5.0×10^{-4}	3.4×10^{-3}	9.5×10^{-3}

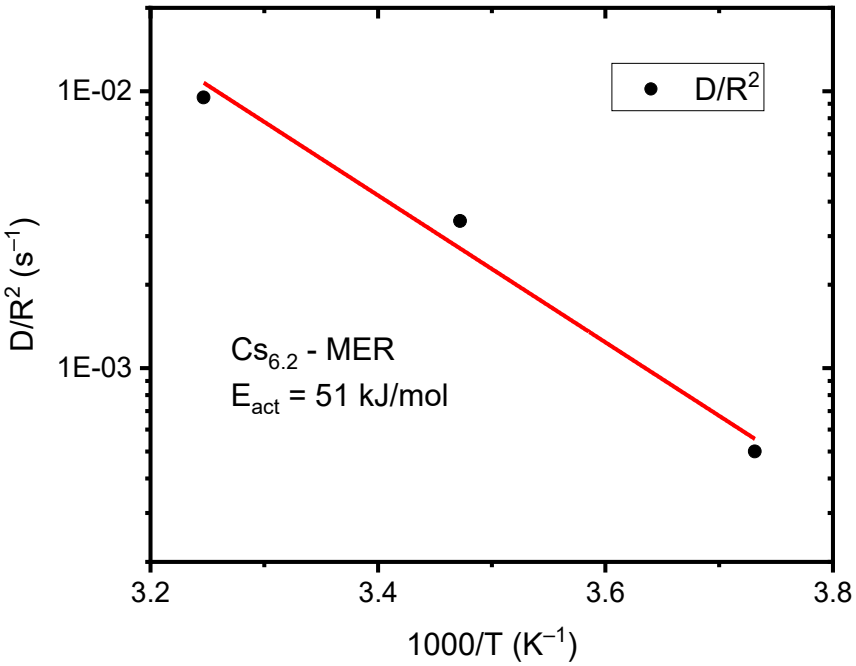

Figure 7.9. Diffusivity values for $Cs_{6.2}$-MER at different temperatures allows for an estimation of its activation energy.

Additionally, for $Cs_{6.2}$-MER, there appears to be a kinetic limitation in transition, as evidenced by a lack of overlap for this point in the eluted volume plots. Hysteresis observed in "equilibrium" isotherms would be in agreement with a slow transition.

S 7.2 Beaded samples of $K_{6.2}$-MER

ZLC analysis was carried out on $K_{6.2}$-MER prepared in the larger 2 mm diameter beads, with 35.5% Al_2O_3 binder, as described in the experimental section. Analysis was carried out on the bead form as for the powder samples. The normalised concentration, c/c_0, against eluted volume at 308 K in 0.1 bar CO_2 in helium at ambient pressure is shown in Figure S. The q_0 of this material is *ca*. 2.7 mol/kg of MER, higher than observed for the powder form of the material. Minor kinetic limitations are apparent from slight deviations between different flow rates and suggests the introduction of macropores.

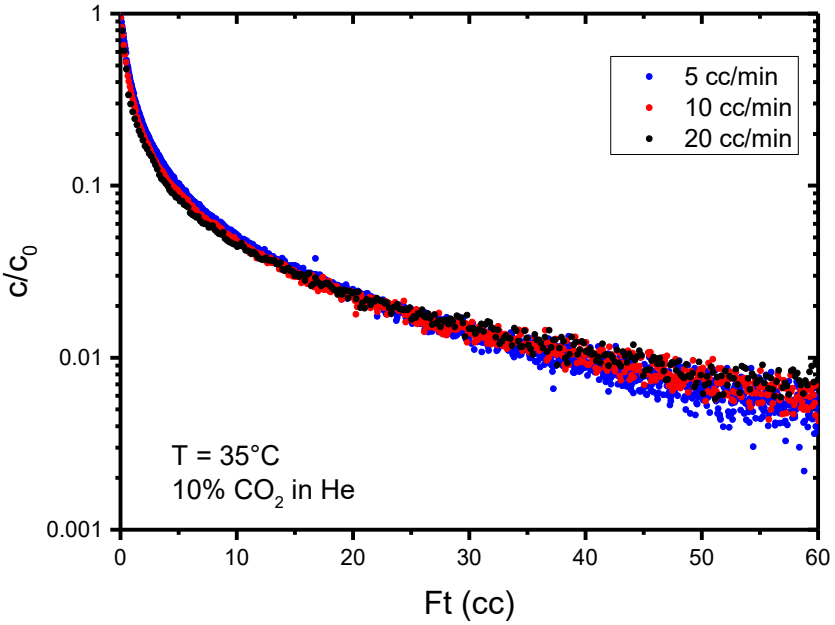

Figure S7.10 Normalised concentration c/c_0 vs. eluted volume for $K_{6.2}$-MER (2 mm beads).

The effective macropore diffusivity can be determined through our ZLC analysis, fitting with an analytical model at varying flow rates, as shown in Figure S. This gave $D_{eff}/R^2 = 9.0 \times 10^{-4}$ s^{-1}.

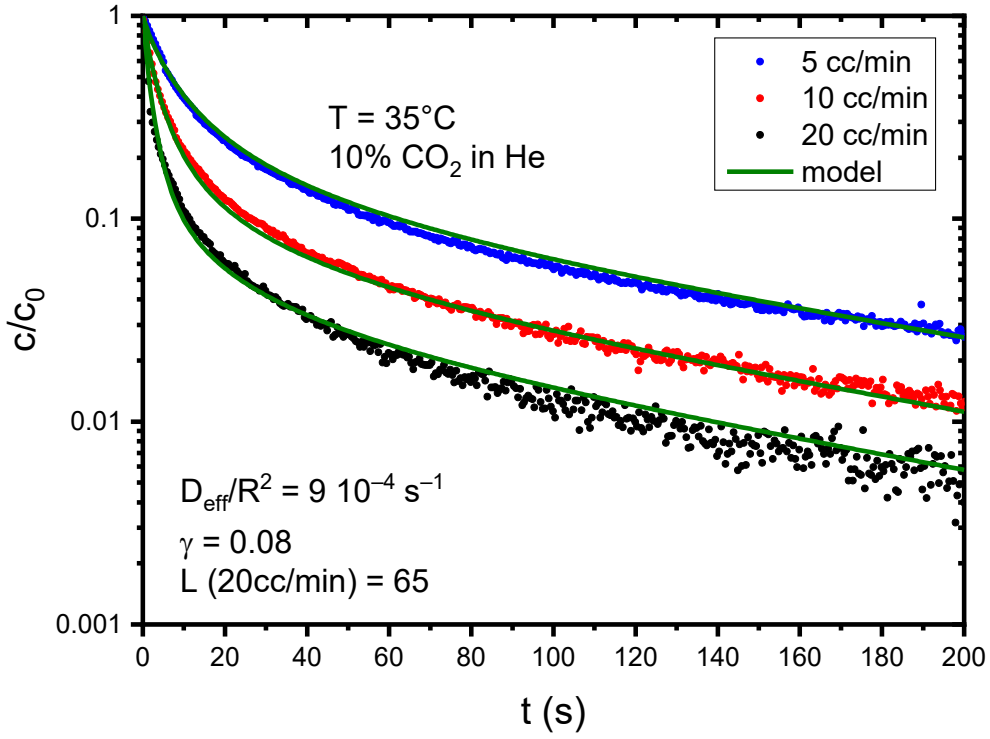

Figure S7.11. Normalised concentration c/c_0 vs. time for $K_{6.2}$-MER. A range of flow rates is shown including fits using an analytic model.

S8 CO_2/CH_4 separation and breakthrough curves

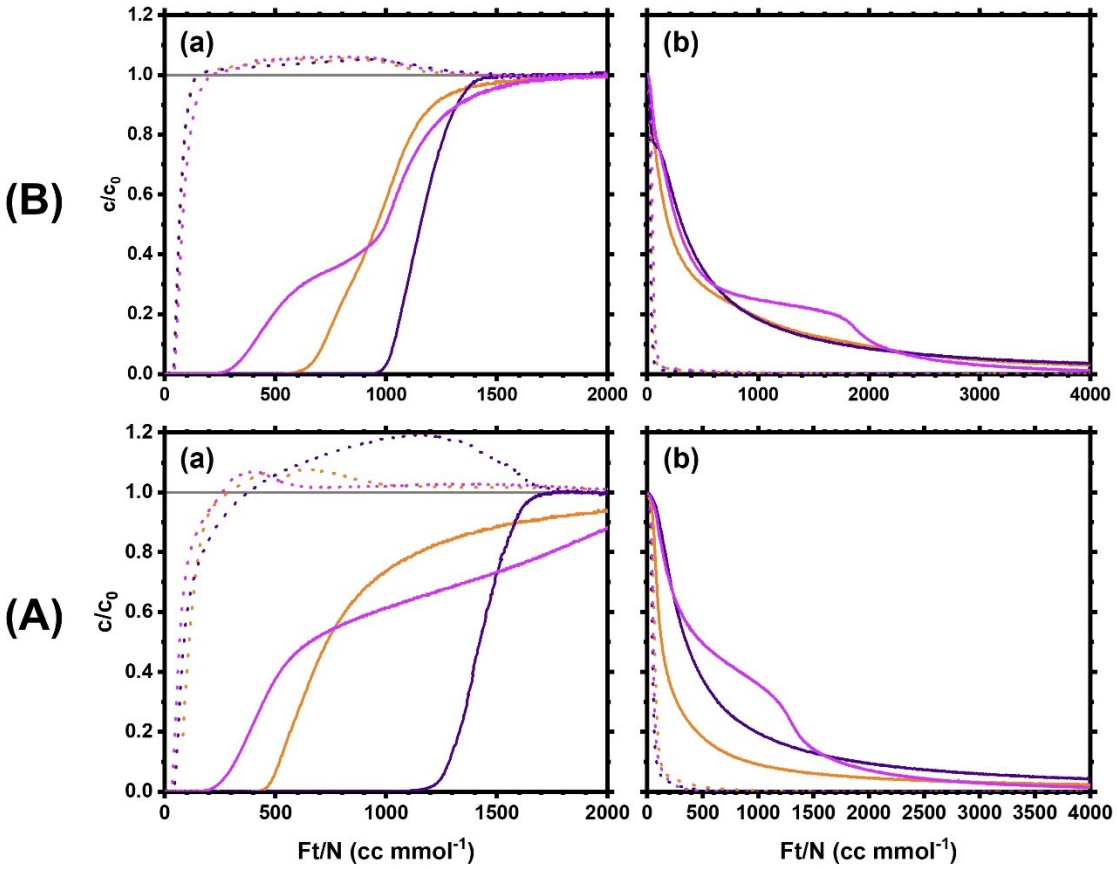

Figure S8.1. Breakthrough (a) adsorption and (b) desorption curves for MER materials: (A) Si/Al = 3.8, 298 K and (B) Si/Al = 4.2, 308 K. CO_2 and CH_4 data is indicated by solid and dotted lines, with Na-, K- and Cs-form data shown in orange, purple and pink, respectively.

S9 Calculating the isosteric heat of CO_2 adsorption, q_{ads}

The heat of adsorption at zero coverage, q_{ads}, for $K_{6.2}$-MER was determined using ZLC data. As was discussed, this material was too rapid for kinetic measurement using ZLC as all adsorption was carried out under equilibrium control, hence the ability to use this data for determination of q_{ads}. Henry's law constants were obtained for 3 temperatures (T = 288, 308 and 328 K) from ZLC uptake data, as shown in Figure S9.1 are listed in Table S9.1.

Table S9.1. Values of Henry's law constants with varying T, calculated from ZLC data.

***T* (K)**	***K* (mol kg^{-1} bar^{-1})**
288	990
308	400
328	165

Figure S9.1. ZLC uptake data, with uptake in mol kg^{-1} plotted against pressure. Blue points show measured values whilst orange points indicates values based on K values.

Plotting ln(K) against T^{-1}, shown in Figure , and multiplying the gradient by the gas constant, R, gives q_{ads} = 35 $\pm$ 1 kJ mol^{-1}. This value is similar to values for K-forms of other zeolites Y, and L, which were found to be 34 - 39 and *ca.* 35 kJ mol^{-1}, respectively.[4,5]

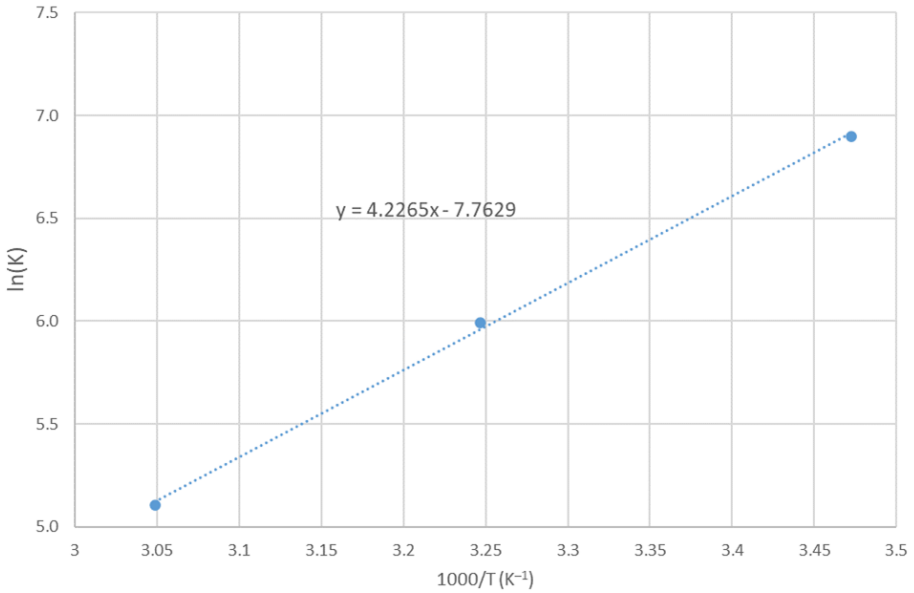

Figure S9.2. Plot of ln(K) against T^{-1} allows determination of q_{ads}.

This value was validated by analysis of CO_2 adsorption isotherms collected at varying temperatures. Fitting the isotherms in Origin software with a Freundlich-Langmuir model,[6] following the approach suggested by Nuhnen and Janiak,[7] such that:

$$n = \frac{a.b.P^c}{1+b.P^c} \quad (1)$$

gives fits shown in Figure S9.3 and variables listed in Table S9.2, although there were few data points at low pressures and uptakes below 2 mmol g^{-1}

Table S9.2. Refined parameters for Freundlich-Langmuir fits of CO_2 adsorption isotherms on $K_{6.2}$-MER at various temperatures.

***T* (K)**	***a***	***b***	***c***
298	9.69	10.47	10.39
308	4.83	2.87	2.04
328	0.49	0.44	0.48

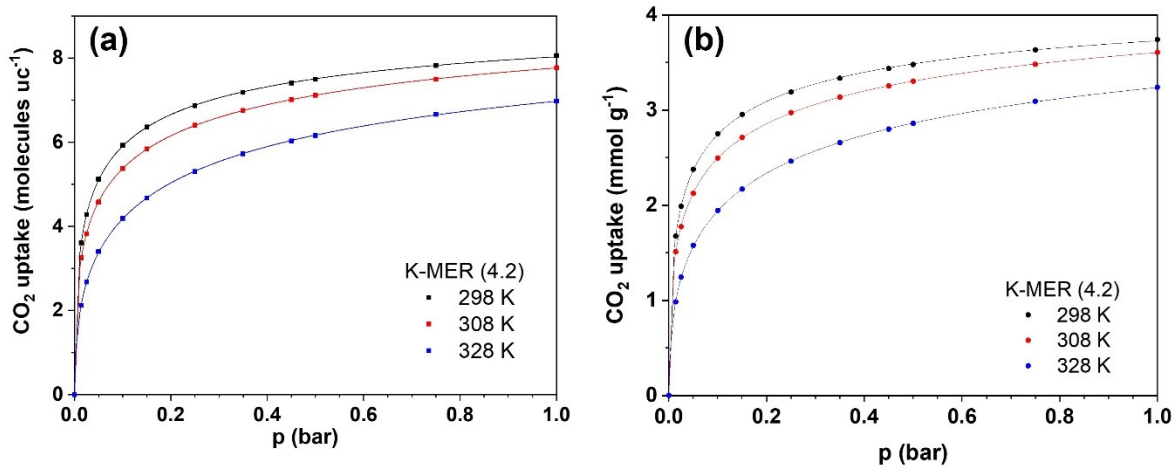

Figure S9.3. CO_2 sorption isotherms at various temperatures and their fits, with uptake in (a) molec uc^{-1} and (b) mmol g^{-1}. Raw data and fits are shown by points and lines, respectively.

Using these fits, plotting ln(P) against T^{-1}, examples of which are shown in Figure S9.4, and again multiplying the gradient by R, gives values of q_{ads} at varying uptakes, from 40 kJ mol^{-1} at 2 mmol g^{-1} to 32.5 kJ mol^{-1} at 3.5 mmol g^{-1} . These values are similar to that obtained *via* ZLC analysis (35 ± 1 kJ mol^{-1}).

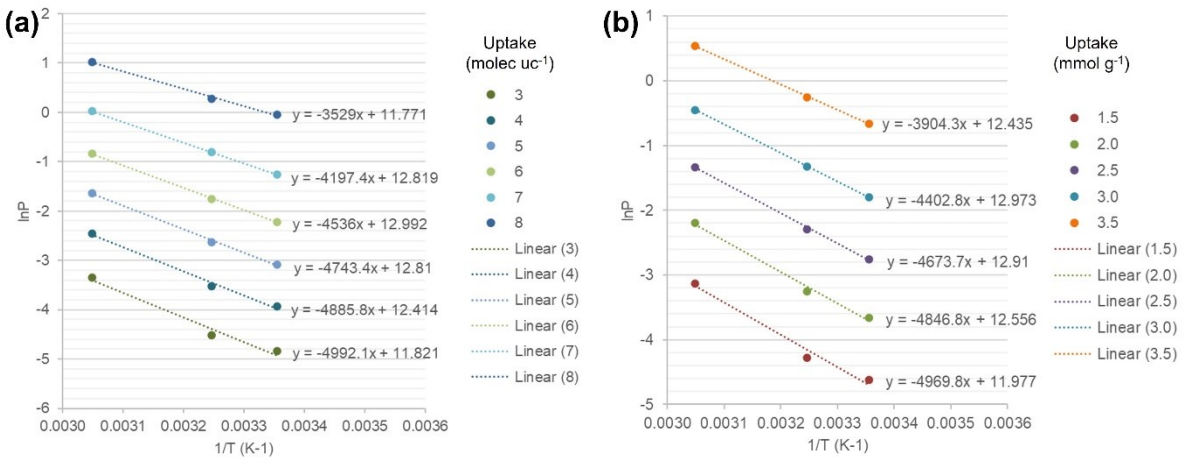

Figure S9.4. Plots of lnP against T^{-1} allows determination of q_{ads}. Data series labels indicate uptake in units of (a) molec uc^{-1} and (b) mmol g^{-1}. It can be seen that the expected linear fit is poor at low uptake values, due to few points on the adsorption isotherm at low pressure.

S10 XRD patterns of $K_{6.2}$-MER/alumina hydrate pellet mixture

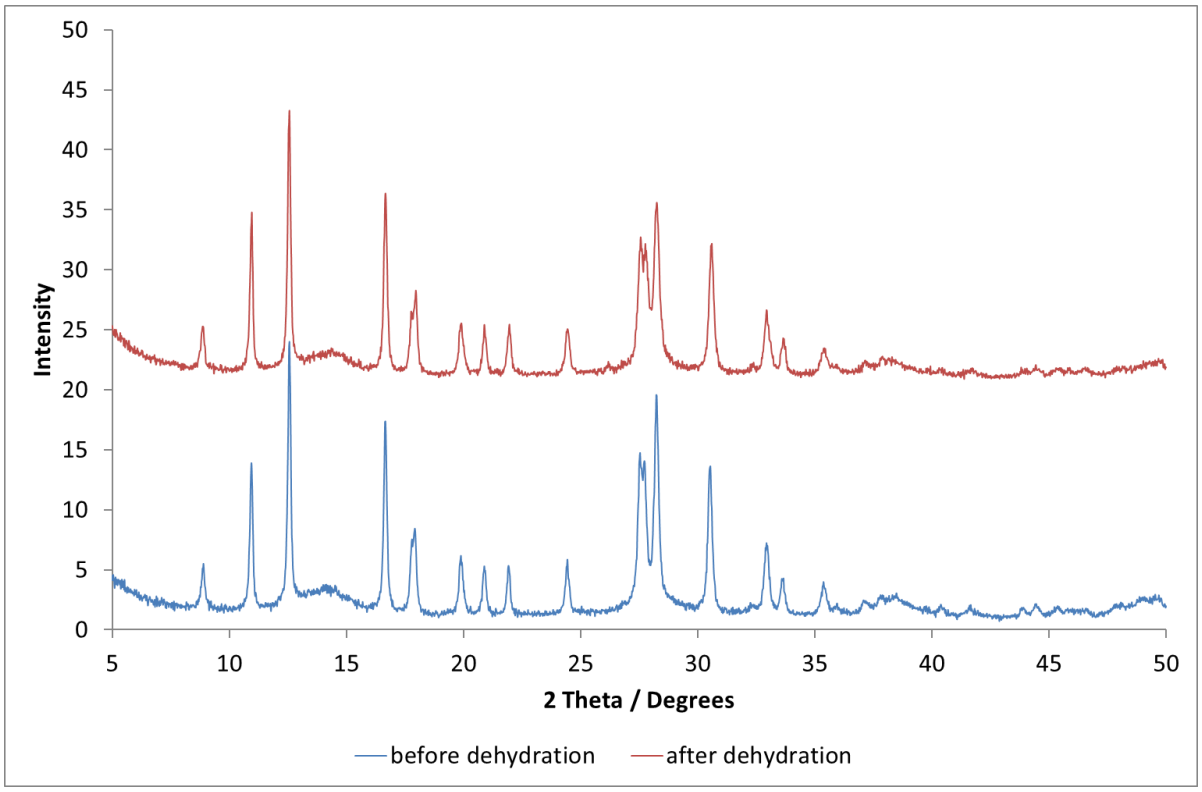

Figure S10.1. XRD patterns of $K_{6.2}$-MER/alumina hydrate pellet mixture before and after calcination

References

(1) Georgieva, V. M.; Bruce, E. L.; Verbraeken, M. C.; Scott, A. R.; Casteel, Jr, W. J.; Brandani, S.; Wright, P. A. Triggered Gate Opening and Breathing Effects during Selective CO_2 Adsorption by Merlinoite Zeolite. *J. Am. Chem. Soc.* **2019**, *141*, 12744–12759.

(2) Eic, M.; Ruthven, D. M. A New Experimental Technique for Measurement of Intracrystalline Diffusivity. *Zeolites* **1988**, *8*, 40–45.

(3) Brandani, S.; Ruthven, D. M. Analysis of ZLC Desorption Curves for Gaseous Systems. *Adsorption* **1996**, *2*, 133–143.

(4) Pirngruber, G. D.; Raybaud, P.; Belmabkhout, Y.; Čejka, J.; Zukal, A. The Role of the Extra-Framework Cations in the Adsorption of CO_2 on Faujasite Y. *Phys. Chem. Chem. Phys.* **2010**, *12*, 13534–13546.

(5) Lozinska, M. M.; Miller, D. N.; Brandani, S.; Wright, P. A. Hiding Extra-Framework Cations in Zeolites L and y by Internal Ion Exchange and Its Effect on CO_2 Adsorption. *J. Mater. Chem. A* **2020**, *8*, 3280–3292.

(6) OriginPro, 2019b (Academic), OriginLab Corporation: Northampton, MA, USA 2019.

(7) Nuhnen, A.; Janiak, C. A Practical Guide to Calculate the Isosteric Heat/Enthalpy of Adsorption *via* Adsorption Isotherms in Metal-Organic Frameworks, MOFs. *Dalt. Trans.* **2020**, *49*, 10295–10307.

(8) Choi, H. J.; Jo, D.; Min, J. G.; Hong, S. B. The Origin of Selective Adsorption of CO_2 on Merlinoite Zeolites. *Angew. Chemie - Int. Ed.* **2020**, *60*, 4307–4314.